Sulfur, Chlorine, & Argon Abundances in Planetary Nebulae. I: Observations and Abundances in a Northern Sample

K.B. Kwitter[1]

Department of Astronomy, Williams College, Williamstown, MA 01267; kkwitter@williams.edu

and

R.B.C. Henry[1]

Department of Physics & Astronomy, University of Oklahoma, Norman, OK 73019; henry@mail.nhn.ou.edu

ABSTRACT

This paper is the first of a series specifically studying the abundances of sulfur, chlorine, and argon in Type II planetary nebulae (PNe) in the Galactic disk. Ratios of S/O, Cl/O, and Ar/O constitute important tests of differential nucleosynthesis of these elements and serve as strict constraints on massive star yield predictions. We present new ground-based optical spectra extending from 3600-9600Å for a sample of 19 Type II northern PNe. This range includes the strong near infrared lines of [S III] $\lambda\lambda$9069,9532, which allows us to test extensively their effectiveness as sulfur abundance indicators. We also introduce a new, model-tested ionization correction factor for sulfur. For the present sample, we find average values of S/O=1.2E-2±0.71E-2, Cl/O=3.3E-4±1.6E-4, and Ar/O=5.0E-3±1.9E-3.

Subject headings: ISM: abundances – planetary nebulae: general – planetary nebulae: individual (IC 5217, M1-50, M1-54, M1-57, M1-74, M1-80, M3-15, NGC 3587, NGC 6309, NGC 6439, NGC 6572, NGC 6790, NGC 6879, NGC 6884, NGC 6886, NGC 6891, NGC 6894, NGC 7026, Pe1-18) – stars: evolution – stars: nucleosynthesis

---

1. Introduction

As a galaxy evolves chemically, interstellar gas is cycled through stars and becomes enriched with metals as these stars convert hydrogen and helium into heavier elements via nuclear processing. Much of our understanding of this whole scheme comes about through the interplay between model-predicted and observed heavy element abundance ratios as a function of some gauge (e.g., metallicity) of the extent to which a system has evolved.

The chemical evolution models that are used to interpret observed abundance data rely sensitively on predicted stellar production rates, or yields, of individual heavy elements, and these rates are in turn inferred from detailed stellar evolution models. Current examples of stellar models with yield predictions include those by Woosley & Weaver (1995), Maeder (1992), and Nomoto et al. (1997a) for massive stars, and by Marigo et al. (1998) and van den Hoek & Groenewegen (1997) for intermediate mass stars. Each of these teams uses state-of-the-art stellar physics, along with poorly constrained assumptions about mixing length, convective overshooting, and mass loss, to predict the new amounts of numerous isotopes that are added to the interstellar medium through winds, supernovae, and planetary nebulae as stars evolve and perish.

Model predictions of heavy element abundance ratios as functions of metallicity are subsequently compared with observations of these same ratios in either the interstellar medium or in stars. Assessing the success of different theoretical stellar yield predictions with observations sharpens our understanding of production rates of heavy elements. Interstellar medium abundances from, e.g., H II regions, testify to the current chemical composition at particular locations in the Galaxy. Stellar abundances archive the composition of the places and times of their formation. Planetary nebulae (PNe) are especially useful because they can be used to infer both current and past compositions: some of their element abundances can be altered by nucleosynthesis in the progenitor; other elements, impossible to make or destroy in the conditions within the progenitor core or envelope, should remain at original stellar birth levels. Thus, abundance studies of PNe originating from stars representing different epochs can reveal an evolutionary picture of how element ratios have changed over time.

One important method for testing nucleosynthetic theory is to look at the evolutionary change of one heavy element with respect to another. In interstellar abundance studies, O/H is almost always taken as the gauge of metallicity, and so abundance ratios such as S/O become measures not of absolute metallicity changes but of differential changes between two elements as chemical evolution progresses.

The use of PNe to measure the original stellar abundances of elements such as sulfur is possible because PN progenitors, intermediate-mass stars with masses between 1-8 $M_{\odot}$, lack sufficient mass to synthesize them, and thus the levels found in the material shed by the dying star to form the nebula are a measure of what was present in the interstellar material when the star itself formed.

This paper is the first in a series of five that strives to test differential nucleosynthesis pre-

dictions for oxygen, sulfur, chlorine, and argon by measuring the abundances of these elements in a large sample (>60 objects) of PNe residing in the Galactic disk and that together represent a significant range in galactocentric distance. The latter point means that, because of the metallicity gradient in the disk, we can explore objects over a modest range in metallicity as measured by O/H, and discover whether the ratios of S/O, Cl/O, and Ar/O behave according to predictions. Various aspects of the abundances of these elements have been explored by other authors including Aller & Czyzak (1983), Aller & Keyes (1987), Barker(1978a,b), Dennefeld & Stasińska (1983), Dinerstein (1980), Freitas-Pacheco (1993), Freitas-Pacheco, Maciel, & Costa (1992), Kingsburgh & Barlow (1994), Köppen, Acker, & Stenholm (1991), Maciel & Köppen (1994), Maciel & Chiappini (1994), Maciel & Quireza (1999), and Peimbert & Torres-Peimbert (1987).

Our survey includes the important near-infrared (NIR) emission lines of [S III] $\lambda\lambda 9069,9532$. Pioneering work on observing [S III] in PNe was carried out by Barker (1978b, 1980b, 1983) and by Dinerstein (1980), both of whom used a photoelectric scanner to measure $\lambda 9532$ at ~ 20Å resolution. We are able to take advantage of the improvement in detector technology to achieve spatial resolution that measures precisely the same region in the nebula in the NIR as in the optical, as well as spectral range that enables observation of both $\lambda 9069$ and $\lambda 9532$ (see section 3), and spectral resolution that allows separation of $\lambda 9532$ from Paschen 8 at $\lambda 9546$.

Here we present new spectrophotometric measurements of 19 northern hemisphere Type II PNe between 3600-9600Å. Type II PNe were chosen because there is substantial evidence through their kinematics that these objects are part of a young population orbiting very near the plane of the Galactic disk (Peimbert 1990). At the same time, their progenitor stars are considered to be of insufficient mass to allow oxygen depletion or neon enrichment (through ON cycling or carbon burning, respectively) during the star's life. Hence they provide current measurements of interstellar abundances in the disk.

Using 5-level atom routines along with model-tested ionization correction factors for certain elements, we calculate and report the nebular abundances of He, N, O, Ne, S, Cl, and Ar in 18 objects. (For one of the 19 observed PNe, NGC 6894, we did not detect measureable [O III] $\lambda 4363$, and so we could not perform a complete abundance analysis.) We focus in particular on the resulting abundance ratios of S/O, Cl/O, and Ar/O. Combining $\lambda\lambda 9069,9532$ with the $\lambda 6312$ auroral line of [S III], we are able to derive a [S III] temperature to measure abundances of S^{+2}. Our hope is to verify or improve upon the S abundances heretofore determined using only the more accessible but weaker [S III] $\lambda 6312$ line to derive S^{+2}. We also introduce a new model-tested ionization correction factor for sulfur, derived in light of new atomic data and sensitive to matter-boundedness.

Papers IIa and IIb in the series are a continuation of our study, using a sample of 48 southern hemisphere Type II PNe; the former will present the observations, the latter will describe the abundance analysis. Paper III will present abundance results for Type II PNe with available ISO mid-IR fine-structure lines of S^{+3}. Paper IV will present new S, Ar, and Cl abundances for a set of Type II PNe whose other abundances were included in a previous series of papers. Finally, Paper V

will make use of all of our amassed data plus information on planetary nebula distances to interpret our derived abundance ratios in light of published stellar yields and our own chemical evolution models. One principal goal of our study is to look for the signature of contributions from Type Ia supernovae, which, according to models by Nomoto et al. (1997b), generate a significant amount of S, Cl, and Ar per event. While the rate of Type Ia events is thought to be several times below that of Type II events (Cappellaro, Evans, & Turatto 1999), we would like to ascertain whether the former objects do, in fact, play an important role in the chemical evolution of S, Cl, and Ar.

The organization of this paper is as follows. Section 2 contains a discussion of the spectral data, including a sample plot with important line identifications, and our reported line strengths. Section 3 discusses our methods for deriving the ionic and elemental abundances and includes comparisons and plots of our results. Section 4 is a summary of our findings for this sample of objects.

2. Observations and Reductions

2.1. Observations

Observations were obtained at KPNO during 1999 28 June - 1 July using the Goldcam CCD spectrometer attached to the 2.1m telescope. The chip was a Ford 3K × 1K CCD with 15μ pixels. We used a slit that was $5''$ wide and extended $285''$ in the E-W direction, with a spatial scale of $0{.}''78$/pixel. With a combination of two gratings, we obtained spectral coverage from 3700-9600Å with overlapping coverage from $\sim$5750 - 6750Å. Using grating #240 with a WG 345 order-separation filter, wavelength dispersion was 1.5 Å/pixel ($\sim$8 Å FWHM resolution) for the blue. For the red we used grating #58 with an OG530 order-separation filter, yielding 1.9 Å/pixel ($\sim$10 Å FWHM resolution). Table 1 lists the objects observed, their angular sizes, and the exposure times in seconds for the blue and red grating configurations. Most of these PNe are relatively small in angular size; therefore, we placed the Goldcam slit on the brightest part of the nebula as seen on the acquisition screen, avoiding the central star if it was visible. We obtained the usual bias and twilight flat-field frames each night, along with HeNeAr comparison spectra for wavelength calibration and standard star spectra for sensitivity calibration.

The thinned red chip produces interference fringes visible in the red. In our red spectra the fringes appear at the $\pm1\%$ level at $\sim$7500Å and increase in amplitude with increasing wavelength: $\pm1.5\%$ at 8000Å, $\pm4.5\%$ at 8500Å, $\pm6\%$ at 9000Å. Even at their worst, $i.e.$, at $\sim\lambda9500$, the longest wavelength we measure, the fringe amplitude reaches only about $\pm7\%$, and we note this additional uncertainty in our line intensities longward of $\sim$7500Å.

A typical spectrum is shown in Fig. 1, combined here into a single plot. In this nebula, M1-57, lines from multiple ions of S, Ar, and Cl are identified, along with other important spectral features.

The original spectra were reduced in the standard fashion using IRAF[2]. We used tasks in the *kpnoslit* package to convert these two-dimensional spectra to one dimension by collapsing data along the slit.

2.2.   Line Strengths

Line strengths were measured using *splot* in IRAF and are reported in Tables 2A-D. Fluxes uncorrected for reddening are presented in columns labeled $F(\lambda)$, where these flux values have been normalized to $H\beta=100$ using our observed value of log $F_{H\beta}$ shown in the last row of the table. These line strengths in turn were corrected for reddening by assuming that the relative strength of $H\alpha/H\beta=2.86$ (Osterbrock 1989; Table 4.4) and computing the logarithmic extinction quantity c shown in the penultimate line of the table. Values for the reddening coefficients, $f(\lambda)$, are listed in column (2), where we employed the extinction curve of Savage & Mathis (1979). Intensities are corrected by multiplying the observed ratio relative to $H\beta$ by $\mathrm{dexp}[cf(\lambda)]$. To check the validity of the values of c derived from $H\alpha/H\beta$ we calculated values using the ratio of P10 $\lambda9014$ and P8 $\lambda9546$, each with respect to $H\beta$. Table 3A contains all of the calculated values for c, which are also shown graphically in Fig. 2. As can be seen, the agreement is generally quite good between $H\alpha$ and Paschen extinction c measurements, providing support for our spectrum reduction and merging techniques.

The columns headed $I(\lambda)$ in Tables 2A-D list our final, corrected line strengths, again normalized to $H\beta=100$. In general, intensities of strong lines have measurement uncertainties $\leq10\%$; single colons indicate uncertainties of more than $\sim25\%$, and double colons denote uncertainties exceeding $\sim50\%$.

Finally, as a check on the accuracy of our final line strengths, in Table 3B we compare observed and theoretical values for a number of line ratios which are set by atomic constants. The first column lists the object name while the subsequent seven columns give the observed ratios, where each ratio is defined in the table footnote. The last two rows of the table give the observed mean and standard deviation, and theoretical value of each ratio. Agreement is reasonable for all but the [Ne III] ratio, which may be affected by incomplete subtraction of $H\epsilon$. The closeness of the other ratios to their theoretical values confirms our general claim of line strength uncertainty of $\pm10\%$ for strong and moderately strong lines.

---

[2]IRAF is distributed by the National Optical Astronomy Observatories, which is operated by the Association of Universities for Research in Astronomy, Inc. (AURA) under cooperative agreement with the National Science Foundation.

3. Calculations

3.1. The General Scheme

Electron temperatures and densities, ionic abundances, and total elemental abundances were computed from our measured line strengths using the program ABUN (written by R.B.C.H.), which features a 5-level atom routine along with ionization correction factors (ICF) either taken from the literature or derived below. Table 4 summarizes the ions observed, the wavelengths of the emission lines used to obtain ionic abundances, temperatures, and densities, and the sources of the atomic data used in ABUN.

Ionic abundances are calculated directly from line strengths; the former are then added together and their sum multiplied by an appropriate ICF, i.e., the ratio of total elemental abundance to the sum of observable ions, to correct for unseen ions. This procedure can be expressed analytically for the number abundance of element X as follows:

$$N(X) = \left\{ \sum^{obs} \frac{I_\lambda}{\epsilon_\lambda(T_e, N_e)} \right\} \cdot ICF(X). \tag{1}$$

Since we are generally interested in determining ionic abundances with respect to H^+, I_λ is entered as a value which has been normalized with respect to $H\beta$, and hence an $H\beta$ generation rate is included in the denominator of Eq. 1.

We prefer this approach to modeling each nebula individually using a photoionization code for the following reasons. First, nearly all PNe have irregular geometries which cannot easily be included in such a model. Second, unless the entire nebula lies within the spectroscopic slit, observed lines-of-sight cut through only a portion of the nebula, and the resulting data are not likely to be equivalent to those obtained with whole-nebula observations; photoionization models representing the latter do not necessarily produce line strengths which can be meaningfully compared with observed ones. Third, applying our method to output from a range of photoionization models representing large regions of parameter space returns abundances that are quite consistent with the original model input abundance set. Finally, in previous work (Henry, Kwitter, & Bates 2000; Kwitter & Henry 1996, 1998; Henry & Kwitter 1998; Henry, Kwitter, & Howard 1996), we have carefully modeled individual line-of-sight sections of nebulae and calculated a model-determined correction factor which we then applied to abundances obtained using the standard ICF approach. In nearly all cases these model-determined corrections were found to be minor compared with other sources of uncertainty.

We want to draw particular attention to our use of the NIR lines of [S III] $\lambda\lambda$9069,9532 for determining S^{+2} abundances. It is the use of high-quality measurements of these lines in a large PN sample that distinguishes our study from previous ones that have included sulfur abundance measurements. While these nebular lines are much stronger than the auroral line at λ6312, they

ostensibly suffer from effects of telluric absorption and emission, effects that are extremely difficult to remove. The main problem is that the atmospheric features are molecular in origin (primarily OH) and are often very narrow compared with the widths of the nebular lines, since the latter may be broadened by turbulent motions within the nebula itself. This problem has been extensively analyzed by Stevenson (1994), who proposed a rigorous remedy that includes the use of relatively featureless comparison stellar spectra to determine the location and intensity of each molecular band. However, because such stellar spectra were not available to us, we used the fact that the ratio of the two NIR lines of [S III] is determined by atomic physics, is independent of environment, and is equal to 2.48, based on the S^{+2} atomic data cited in Table 4. Thus, if the observed intensity ratio of $\lambda 9532/\lambda 9069$ in an object was greater than or equal to 2.48, we assumed that the $\lambda 9532$ line was less affected by atmospheric absorption and we used it in the ionic abundance calculation for S^{+2}. Alternatively, when the observed line ratio was less than 2.48, we used the $\lambda 9069$ line for the ionic abundance determination, assuming it to be the less affected.

Corrected line strengths from Table 2A-D were read into ABUN and calculations were made as follows. Electron temperatures and densities were calculated in the standard fashion using ratios of lines from auroral and nebular transitions sensitive to temperature, density, or both. Abundances of observed ions were calculated by dividing the energy production rate per ion at the observed wavelength $\epsilon_\lambda(T_e, N_e)$ into the observed line intensity I_λ for each of the emission lines listed in Table 4. In calculating ionic abundances, the [O III] temperature was used for the high ionization species (O^{+2}, Ne^{+2}, Cl^{+2}, Cl^{+3}, Ar^{+2}, and Ar^{+3}), the [N II] temperature was used for the low ionization species (O^o, O^+, N^+, and S^+), and the [S III] temperature was used for S^{+2}. The sum of observed ions of one element was then multiplied by the appropriate ICF, as shown in eq. 1.

3.2. Ionization Correction Factors

ICFs for He, O, N, Ne, and Ar have been reasonably well established by numerous investigators in the past. After testing candidates with photoionization models, we are convinced that the ICFs for these elements reported by Kingsburgh & Barlow (1994) in their study of abundances in southern PNe provide reliable results, so we have adopted them for determining final elemental abundances below.

3.2.1. The Ionization Correction Factors for Sulfur and Chlorine

The ICF for sulfur is a different matter. Initial attempts to devise such a factor were based primarily on the fact that ionization potentials for S^{+2} and O^+ are nearly the same, i.e. 35.1eV and 34.8eV, respectively. Hence, Peimbert & Costero (1969) used

$$S/H = \frac{S^+ + S^{+2}}{H^+} \frac{O}{O^+},$$
(2)

where each atom or ion symbol represents a number abundance. The second fraction on the right hand side is the sulfur ionization correction factor ICF(S) when lines of both S^+ and S^{+2} are observed. This form was later employed by Barker (1978b), but Barker, as well as Pagel (1978), noticed that when this form was used, resulting S/H ratios increased systematically with O/O^+, indicating the occurrence of an overcorrection for unobserved S^{+3} when the O/O^+ ratio is relatively large, e.g. in highly ionized and/or matter-bounded nebulae.

Stasińska (1978), in a study of H II regions, was the first to use photoionization models to derive a correction factor, the form of which is:

$$\mathsf{ICF(S)} = [1 - (\mathsf{O^+/O})^\alpha]^{-1/\alpha}, \tag{3}$$

where $\alpha = 3$. French (1981) employed this form in a study of PNe, but favored $\alpha = 2$, a value subsequently adopted by Dennefeld & Stasińska (1983) in another H II region study following an analysis based upon an updated model grid by Stasińska (1982) which this time included the effects of charge exchange on the ionization structure of sulfur. Garnett (1989) also calculated a separate photoionzation model grid for a study of H II regions and found a behavior for ICF(S) which fell between the curves for $\alpha = 2$ and $\alpha = 3$. Finally, two papers determined the abundance of the S^{+3} ion, the principal unseen species. Natta, Panagia, & Preite-Martinez (1980) used photoionization and recombination cross-sections then available to calculate the ratio of S^{+3}/S^{+2} by assuming ionization equilibrium and obtaining the value of the denominator directly from observations. On the other hand, Dinerstein (1980) observed the S^{+3} ion abundance directly by measuring [S IV] 10.5μm in a sample of 12 PNe and found that using O/O^+ as the ICF(S) overpredicted the S^{+3} abundance.

We felt there was a need to reexamine the ICF(S) issue primarily because of changes in atomic data for sulfur. First, state-of-the-art photoionization cross-sections (Verner et al. 1996), which are based upon the results of the Opacity Project (Seaton et al. 1992) have nearly doubled for energies slightly above threshold for the S^+ and S^{+2} ions since the early values computed by Chapman & Henry (1971) were employed by Stasińska (1978, 1982). Of course radiative recombination rates which are based upon these cross-sections have also changed. Second, charge exchange rates appear to rival those of radiative recombination. For example, using rate coefficients from Butler & Dalgarno (1980) for the reaction $S^{+3} + H^o \rightarrow S^{+2} + H^+$, radiative recombination rates from Aldrovandi & Pequignot (1973), and assuming that the ratio of electron density to H^o density is 10^3 (typical for ionized nebulae), we find that the rates are roughly equal, and so it is imperative that charge exchange be included in the development of ICF(S). Both Stasińska (1982) and Garnett (1989) used the Butler and Dalgarno charge exchange rates in their models, although the effects of this process were not, of course, part of the ICF(S) which was based simply on ionization potentials (eq. 2), and used in the early work on sulfur. Finally, there is the problem introduced by dielectronic recombination (DR) reactions involving complex ions such as those of sulfur. Essentially, DR for sulfur is the wild card in the analysis (G. Ferland, private communication), and the situation is discussed in Ali et al. (1991). Although low-temperature rates have yet to be calculated for ions of sulfur, the photoionization model code CLOUDY (Ferland 1996) contains estimated cross-sections

and allows rough estimates of the effects of DR to be made. We ran two models, both for stellar effective temperature of 100,000K, total density of 1000 cm^{-3}, and solar abundances. One model included DR in the calculation, while the other did not. We found that the fraction of sulfur in the S^+ and S^{+2} stages increased by 34% and 14%, respectively, when DR was part of the calculation, and thus the ICF(S) would be expected to be significantly lower when this process is included.

We therefore have carried out our own investigation of ICF(S) by calculating a new grid of photoionization models using CLOUDY version 94. We computed models with central star blackbody effective temperatures of 35,000K, 50,000K, 75,000K, 100,000K, and 150,000K, and for each of these temperatures we employed two density regimes, 10 cm^{-3} and 1000 cm^{-3}. For each temperature-density combination we calculated several models which covered a range of matter-boundedness. Elemental abundances were set at solar values in all cases. Each model included up-to-date atomic data as well as effects of charge transfer and dielectronic recombination processes, most notably those relevant to ions of sulfur.

Values of $S/(S^++S^{+2})$ and O/O^+ for each model were formed by extracting the relative ionic abundances for S^+, S^{+2}, and O^+ over the entire nebula from the output of each model and combining these results with the input elemental abundances for S and O. Fig. 3 is a logarithmic plot of the first ratio, which equals the ICF(S), against the second one, where each open circle represents one model from our grid. The solid line shows a third order fit through the points with the form $ICF(S) = dexp[-.017+(.18\times\beta)-(.11\times\beta^2)+(.072\times\beta^3)]$, and $\beta = \log(O/O^+)$. The solid horizontal line toward the top of the graph indicates the range of the observed values of $\log(O/O^+)$ in our PN sample. The curves that result from using the ICF(S) expressions given by Peimbert & Costero (1969; eq. 2 above; dot-dashed line), French (1981; dotted line; eq. 3 with $\alpha = 2$) and Stasińska (1978; dashed line; eq. 3 with $\alpha = 3$) are also shown in Fig. 3 for comparison. It would appear that the Stasińska expression is similar to ours, although at large O/O^+ values even that relation will tend to overestimate ICF(S) and produce systematically larger values for S abundances relative to our scheme. This result is probably due to the estimated effects of DR which are included in our analysis for the first time. In our abundance calculations for S to follow, we use our analytical fit given above as the expression for ICF(S).

Obtaining a suitable ICF for chlorine proved to be a more straightforward task than the one just described for sulfur. By studying the ionization structure of our models we found that the observed ions of Cl^{+2} and Cl^{+3} roughly coexist with He^+, and thus $Cl/(Cl^{+2}+Cl^{+3})=He/He^+=ICF(Cl)$ seems appropriate. We adopt this form in the abundance calculations below.

We now summarize the ICFs we employed in our analysis:

$$ICF(He) = \frac{He}{He^+ + He^{+2}} = 1.0, \tag{4a}$$

$$ICF(O) = \frac{O}{O^{+2} + O^+} = \frac{He^+ + He^{+2}}{He^+}, \tag{4b}$$

$$\text{ICF(N)} \quad = \quad \frac{N}{N^+} = \frac{O^+ + O^{+2}}{O^+} \times \frac{He^+ + He^{+2}}{He^+}, \tag{4c}$$

$$\text{ICF(Ne)} \quad = \quad \frac{Ne}{Ne^{+2}} = \frac{O^+ + O^{+2}}{O^{+2}} \times \frac{He^+ + He^{+2}}{He^+}, \tag{4d}$$

$$\text{ICF(S)} \quad = \quad \frac{S}{S^+ + S^{+2}} = \text{dexp}[-.017 + (.18 \times \beta) - (.11 \times \beta^2) + (.072 \times \beta^3)], \tag{4e}$$

$$\text{ICF(Cl)} \quad = \quad \frac{Cl}{Cl^{+2} + Cl^{+3}} = \frac{He^+ + He^{+2}}{He^+}, \tag{4f}$$

$$\text{ICF(Ar)} \quad = \quad \frac{Ar}{Ar^{+2} + Ar^{+3}} = \frac{1}{1 - \frac{N^+}{N}} \times \frac{He^+ + He^{+2}}{He^+}, \tag{4g}$$

where $\beta = \log(O/O^+)$ in eq. 2e. Also, when $\log(O/O^+) \leq +0.6$, our model tests suggested that $Ar/Ar^{+2}=1$, and so we used this relation to obtain elemental argon abundances under that condition.

Finally, we tested our abundance methods by comparing model input abundances with derived abundances for S, Cl, and Ar, the elements we are focusing on in this paper. To accomplish this, we used ABUN, including the ICFs listed above, to calculate abundances based on the output line strengths in our grid. We then divided each derived abundance into the input abundance set in the same model. These quantities are then plotted logarithmically in Fig. 4 against central star temperature for the radiation-bounded models calculated out to the Strömgren radius (solid lines) as well as the matter-bounded ones calculated out to a distance of one-half the Strömgren radius (dashed lines). If our scheme were perfect, lines in all panels would be exactly horizontal at a constant ordinate value of zero. With a few exceptions, our methods consistently produce abundances for these elements within 0.1 dex of the actual abundance in the model, strongly suggesting that the methods we apply to the data for the PNe in our sample below are reliable.

4. Results

Derived electron temperatures and densities for our objects are listed in the last six rows of Tables 5A-D. Generally speaking, these values are uncertain by $\pm10\%$. Note that in most instances, [O III], [N II], and [S III] temperatures agree closely, indicating that our measurements of the weak auroral lines in those cases were quite good. A few improbable values for temperature and density are enclosed in parentheses; likely causes are measurement uncertainties in the lines used and/or the effect of errors in the reddening correction over a long wavelength baseline.

Abundances for observed ions are reported in Tables 5A-D, along with ICFs for each element. The first column of each table contains the ion ratio or ICF whose value is given in the subsequent columns for the objects shown at the column head. We point out that these are *number* abundance ratios. Also, note that while we observed [Ar V] $\lambda7005$ in most of our objects, its strength is generally very weak, and photoionization models indicate that in PNe Ar^{+4} is not expected to be present at sufficient levels to influence the Ar abundance measurement. Hence, we do not report

an abundance for this ion.

In the case of S^{+2}/H^+, we provide two values. The first one is the value derived using the NIR lines of [S III] $\lambda\lambda$9069,9532 (as described in §3), while the second one is derived using the [S III] λ6312 line[3]. We note that these two sets of numbers agree well in most cases. Fig. 5 is a plot of S^{+2}/H^+ derived from the λ6312 line versus the same ratio derived from the NIR lines. The diagonal line shows the track for a one-to-one correspondence. Clearly the agreement is good in all but two cases, M1-54 and M1-57, where λ6312 results for $S^{+2}/H^+ \times 10^6$ exceed 10 in Fig. 5. These two discrepancies can be traced to severe blending problems of [O I] λ6300 with [S III] λ6312; in these two objects the ratio of λ6300 to λ6312 is extremely high. Generally, however, the agreement in S^{+2} abundances derived from λ6312 and the NIR lines indicates that the common use of the [S III] λ6312 line in the past for computing sulfur abundances, e.g., Kingsburgh & Barlow (1994), is validated.

Finally, note that in many cases the ICF for nitrogen is very high. This can be directly traced to the relatively large value for the ratio of O/O^+ which is a factor in ICF(N) (see eq. 2C). This is likely due to the fact that these PNe are truncated or matter bounded, causing the O/O^+ ratio to be large, and, likewise N/N^+. This may in turn impact the Ar abundances through ICF(Ar), causing the former to be underestimated in these cases.

Elemental abundances with respect to H^+ and O are reported in Tables 6A-D. Note that the last two columns of Tables 6 contain abundances measured in the Sun by Grevesse et al. (1996) and in the Orion Nebula by Esteban et al. (1998) for purposes of comparison.

Many of our objects are included in the abundance compilation published by Maciel & Köppen (1994), and comparing our observed line intensities with those from sources listed in that paper reveals good agreement in general. Variations in ionic abundances provided in those same sources can at least partially be be accounted for by differences in the adopted values of the reddening constant, c, and in the extinction functions employed. For example, at moderate reddening, given equal λ3727/Hβ flux ratios, a difference of 0.25 in the value of c and of 0.025 in the value of f(λ) can produce a difference of $\sim$20% in the corrected intensity ratio and thus in O^+/H^+ abundance. Similarly, for equal λ9532/Hβ ratios, a difference of 0.25 in c and of 0.08 in f(λ) can yield a corrected intensity ratio and inferred S^{+2}/H^+ abundance different by $\sim$65%.

Our final abundances as listed in Table 6A-D agree well with previous determinations, almost exclusively within the quoted errors. For example, our values for NGC 6439 and IC 5217 are quite close to those determined by Freitas-Pacheco, Maciel & Costa (1992), and by Hyung et al. (2001), respectively. Disagreements in other cases may be due to analytical differences, as described above, as well as to limitations in the spectral resolution and range of previous observations.

---

[3]Note that the [N II] temperature was employed when S^{+2} was derived from the λ6312 line, whereas the [S III] temperature was used in association with the NIR lines, as mentioned in §3.1

While we are postponing a detailed analysis of our derived abundances until Paper V of this series when the results of the entire sample are available, we present abundance results for S/O, Cl/O, and Ar/O for our current sample in Fig. 6.[4] The top panel is a plot of S/O versus O/H for our objects. We also show the position of the Sun (Grevesse et al. 1996; star) and the Orion Nebula (Esteban et al. 1998; X) for comparison. The middle and bottom panels share the same format as the top one but for the ordinates, which are, respectively, Cl/O, and Ar/O. A vertical error bar in each panel indicates the ordinate uncertainty, while the horizontal error bar in the top panel serves to show the uncertainty in O/H for all three panels. Table 7 compares arithmetic averages and standard deviations of the abundance ratios in our sample with averages for PN samples reported by Kingsburgh & Barlow (1994) and Aller & Keyes (1987), as well as for the Sun and Orion Nebula.

For S, we see that our average S/O is slightly lower than the findings for the other PN samples as well as for Orion and the Sun. However, our results are consistent with those of Kingsburgh & Barlow, considering the uncertainties associated with both samples. [We also note that Stasińska's expression ($\alpha = 3$) is the one adopted by Kingsburgh & Barlow (1994).] We speculate that systematically lower values for S/O in our sample are at least partially related to our use of an ICF(S) relation (see eq. 2e) that tends to yield corrections that are smaller than those used in the comparison samples and for Orion (see discussion of Fig. 4 above). We mention again that this is perhaps related to the inclusion of dielectronic recombination in the derivation of ICF(S) for the first time. Once accurate cross-sections for this process are available, the behavior of ICF(S) may change significantly, and this fact must be kept in mind when considering our final sulfur abundances presented here.

Final values of Cl/O and Ar/O show greater scatter and larger uncertainty, and this result is undoubtedly related to the fact that generally the line strengths used to determine Cl and Ar abundances are much weaker than those for S. However, our averages for Cl and Ar compare favorably with those listed in Table 7 from the other sources.

5. Summary

We present the first large spectroscopic survey of Type II planetary nebulae in which the spectral range extends from 3600-9600Å. This wide range includes the strong nebular lines of [S III] $\lambda\lambda9069,9532$, allowing us to measure ionic abundances of S^{+2}, and by extension, accurate abundances of elemental S. In addition, most spectra contain lines of [Cl III] $\lambda5537$, [Cl IV] $\lambda8045$,

---

[4]Problems associated with the well-documented discrepancy between abundances derived from forbidden and from permitted lines (see, e.g., Peimbert, Luridiana, & Torres-Peimbert 1995; Mathis, Torres-Peimbert, & Peimbert 1998; Stasińska 1998; Garnett & Dinerstein 2001) are circumvented to a large extent by normalizing S, Cl, and Ar abundances to O, since then we are comparing abundances derived from forbidden lines. Thus, while abundances with respect to H^+ may be affected by this problem, ratios of other metals with respect to oxygen should remain unaffected.

[Ar III] $\lambda 7135$, and [Ar IV] $\lambda 4740$ which allow us to determine elemental abundances of Cl and Ar as well.

The method we used to determine abundances includes a 5-level atom program which determines ionic abundances of observed ions, then applies an ionization correction factor to the sum of these ions to render an elemental abundance. The principal challenge of this research has been to establish a reliable, robust ionization correction factor for S. Using a grid of photoionization models spanning a broad range in stellar effective temperature, nebular density, and degree of matter-boundedness, we established a relation between the ratio of O/O^+ and $S/(S^+ + S^{+2})$ that could be confidently employed in our conversion of ionic abundances to elemental abundances for S. In the same fashion we determined correction factors for Cl and Ar.

In this paper we present our results for 18 PNe, all located in the northern hemisphere. Our abundance results are consistent with general trends seen before in S/O, Cl/O, and Ar/O. We observe slightly lower S/O ratios than do some earlier surveys of PNe and H II regions, although the significance of this difference is questionable because of overall uncertainties in measured abundances. We show that S^{+2} abundances determined using the NIR lines of [S III] are quite consistent with those inferred from the analysis of the [S III] $\lambda 6312$ line. Thus, sulfur abundances in the literature which were derived from only the $\lambda 6312$ line appear to be reliable when this line is well measured. This agreement also implies that simple steps described here to minimize atmospheric absorption effects on the results from the NIR [S III] lines are generally sufficient to allow confident use of these lines.

Table 1.   Object and Exposure Time Data

Object	Angular Diameter ($''$)[1]	Total Blue Exp (sec)	Total Red Exp (sec)
IC 5217	6.6	210	255
M1-50	5.6	420	540
M1-54	13	840	360
M1-57	8.4	720	540
M1-74	5	140	110
M1-80	8	780	660
M3-15	4.2	1200	1500
NGC 3587	170	1200	1500
NGC 6309	15.5	660	780
NGC 6439	5	420	540
NGC 6572	10.8	72	72
NGC 6790	7	105	100
NGC 6879	5	180	135
NGC 6884	6	130	105
NGC 6886	5.5	140	100
NGC 6891	15	150	215
NGC 6894	40	600	960
NGC 7026	20	240	180
Pe1-18	6.8	1980	540

[1]Taken from Acker et al. (1992).

Table 2A.   Line Strengths

Line	f(λ)	IC 5217 F(λ)	IC 5217 I(λ)	M1-50 F(λ)	M1-50 I(λ)	M1-54 F(λ)	M1-54 I(λ)	M1-57 F(λ)	M1-57 I(λ)	M1-74 F(λ)	M1-74 I(λ)
[O II] λ3727	0.29	17.0	20.2	$\cdots$	$\cdots$	120	191	44.0	124	17.0	27.5
He II + H10 λ3797	0.27	4.3	5.1	$\cdots$	$\cdots$	$\cdots$	$\cdots$	$\cdots$	$\cdots$	2.8	4.4
He II + H9 λ3835	0.26	6.0	7.0	5.6	10.1	5.6	8.5	4.6	11.6	4.6	7.1
[Ne III] λ3869	0.25	92.0	107	61.0	107	74.0	111	53.0	129	56.0	84.8
He I + H8 λ3889	0.25	17.0	19.7	9.7	16.9	17.0	25.2	7.2	17.2	8.5	12.7
Hϵ + [Ne III] λ3968	0.22	41.0	46.8	27.0	44.7	33.0	47.2	22.0	48.7	31.0	44.8
He I + He II λ4026	0.21	2.0	2.3	$\cdots$	$\cdots$	2.5	3.5	$\cdots$	$\cdots$	1.9::	2.7::
[S II] λ4072	0.20	1.3::	1.5::	$\cdots$	$\cdots$	7.8	10.7	6.7:	13.4:	2.7::	3.7::
He II + Hδ λ4101	0.19	24.0	26.8	16.0	24.4	21.0	28.4	11.0	21.4	17.0	23.2
He II λ4198	0.16	$\cdots$	$\cdots$	$\cdots$	$\cdots$	$\cdots$	$\cdots$	$\cdots$	$\cdots$	$\cdots$	$\cdots$
C II λ4267	0.14	$\cdots$	$\cdots$	$\cdots$	$\cdots$	$\cdots$	$\cdots$	0.9::	1.5::	$\cdots$	$\cdots$
Hγ λ4340	0.12	43.0	46.3	30.0	39.6	37.0	45.1	25.0	38.8	35.0	42.9
[O III] λ4363	0.12	11.0	11.8	9.8	12.8	5.0	6.0	14.0	21.3	4.8	5.8
He I λ4471	0.09	4.9	5.2	2.9	3.6	5.1	5.9	2.0	2.8	4.6	5.3
He II λ4540	0.07	$\cdots$	$\cdots$	$\cdots$	$\cdots$	0.3::	0.3::	1.6	2.1	$\cdots$	$\cdots$
N III λ4640	0.05	2.1	2.2	3.0	3.3	3.0	3.2	$\cdots$	$\cdots$	$\cdots$	$\cdots$
He II λ4686	0.04	9.3	9.5	22.0	23.9	18.0	19.1	1.8	2.0	$\cdots$	$\cdots$
He I + [Ar IV] λ4711	0.03	5.1	5.2	4.9	5.2	5.0	5.2	5.5	6.1	1.5	1.6
[Ne IV] λ4724	0.03	$\cdots$	$\cdots$	$\cdots$	$\cdots$	$\cdots$	$\cdots$	$\cdots$	$\cdots$	$\cdots$	$\cdots$
[Ar IV] λ4740	0.02	4.5	4.6	5.0	5.3	2.2	2.3	7.0	7.6	1.3	1.3
Hβ λ4861	0.00	100	100	100	100	100	100	100	100	100	100
He I λ4922	-0.02	1.2	1.2	0.7	0.7	1.4	1.4	$\cdots$	$\cdots$	1.3	1.3
[O III] λ4959	-0.03	412	405	541	506	303	289	632	568	355	338
[O III] λ5007	-0.04	1254	1224	1688	1538	922	863	2027	1750	1101	1028
[N I] λ5199	-0.09	0.1::	0.1::	$\cdots$	$\cdots$	14.0	12.2	6.1	4.5	$\cdots$	$\cdots$
He II λ5411	-0.13	1.1	1.0	2.4	1.8	1.6	1.3	7.1	4.4	$\cdots$	$\cdots$
[Cl III] λ5517	-0.16	0.4:	0.4:	0.3::	0.2::	0.7:	0.5:	2.0:	1.1:	$\cdots$	$\cdots$
[Cl III] λ5537	-0.16	0.6:	0.6:	0.8::	0.6::	1.5:	1.2:	2.8:	1.6:	0.5::	0.4::
[O I] λ5577	-0.17	$\cdots$	$\cdots$	$\cdots$	$\cdots$	$\cdots$	$\cdots$	$\cdots$	$\cdots$	$\cdots$	$\cdots$
[N II] λ5755	-0.21	0.9	0.8	0.3	0.2	13.0	9.3	23.0	11.1	2.2	1.6
C IV λ5806	-0.22	$\cdots$	$\cdots$	$\cdots$	$\cdots$	$\cdots$	$\cdots$	$\cdots$	$\cdots$	$\cdots$	$\cdots$
He I λ5876	-0.23	17.2	15.0	23.0	13.7	28.0	19.4	29.0	12.8	25.0	17.1
He II λ6005	-0.26	$\cdots$	$\cdots$	$\cdots$	$\cdots$	$\cdots$	$\cdots$	$\cdots$	$\cdots$	$\cdots$	$\cdots$
He II λ6038	-0.26	$\cdots$	$\cdots$	$\cdots$	$\cdots$	$\cdots$	$\cdots$	$\cdots$	$\cdots$	$\cdots$	$\cdots$
He II λ6074	-0.27	$\cdots$	$\cdots$	$\cdots$	$\cdots$	$\cdots$	$\cdots$	$\cdots$	$\cdots$	$\cdots$	$\cdots$
[Ca V] λ6087	-0.27	$\cdots$	$\cdots$	$\cdots$	$\cdots$	$\cdots$	$\cdots$	8.4	3.2	$\cdots$	$\cdots$
[K IV] λ6101	-0.28	0.1::	0.1::	0.3:	0.2:	0.1:	0.1:	1.8	0.7	$\cdots$	$\cdots$
He II λ6119	-0.28	$\cdots$	$\cdots$	0.4:	0.2:	0.1:	0.1:	0.9	0.3	$\cdots$	$\cdots$
He II λ6172	-0.29	$\cdots$	$\cdots$	$\cdots$	$\cdots$	$\cdots$	$\cdots$	$\cdots$	$\cdots$	$\cdots$	$\cdots$
He II λ6235	-0.30	$\cdots$	$\cdots$	$\cdots$	$\cdots$	$\cdots$	$\cdots$	$\cdots$	$\cdots$	$\cdots$	$\cdots$
[O I] λ6300	-0.31	2.4	2.0	0.7	0.3	35.0	21.2	100.0	33.0	8.0	4.8
[S III] λ6312	-0.32	1.9	1.6	3.1	1.5	5.0	3.0	25.0	8.2	4.6	2.7
Mg II λ6346	-0.32	$\cdots$	$\cdots$	$\cdots$	$\cdots$	$\cdots$	$\cdots$	$\cdots$	$\cdots$	$\cdots$	$\cdots$
[O I] λ6363	-0.32	0.6	0.5	$\cdots$	$\cdots$	12.0	7.1	34.0	10.3	2.4	1.4
He II λ6407	-0.33	$\cdots$	$\cdots$	$\cdots$	$\cdots$	$\cdots$	$\cdots$	$\cdots$	$\cdots$	$\cdots$	$\cdots$
[Ar IV] λ6436	-0.34	$\cdots$	$\cdots$	$\cdots$	$\cdots$	0.3	0.2	6.8	2.1	$\cdots$	$\cdots$
[N II] λ6548	-0.36	11.0	8.9	7.5	3.4	406	229	514	145	22.0	12.2

Table 2A—Continued

Line	f(λ)	IC 5217 F(λ)	IC 5217 I(λ)	M1-50 F(λ)	M1-50 I(λ)	M1-54 F(λ)	M1-54 I(λ)	M1-57 F(λ)	M1-57 I(λ)	M1-74 F(λ)	M1-74 I(λ)
Hα λ6563	-0.36	354	286	641	286	508	286	1022	286	517	286
[N II] λ6584	-0.36	31.0	25.0	21.0	9.3	1272	712	1580	436	67.0	36.8
He I λ6678	-0.38	5.0	4.0	8.0	3.4	9.0	4.9	12.0	3.1	7.6	4.1
[S II] λ6716	-0.39	1.6	1.3	2.0	0.8	70.0	37.8	103	26.3	4.7	2.5
[S II] λ6731	-0.39	3.2	2.5	3.5	1.5	93.0	50.0	179.0	45.2	6.9	3.6
He II λ6891	-0.42	$\cdots$	$\cdots$	0.4	0.2	$\cdots$	$\cdots$	$\cdots$	$\cdots$	$\cdots$	$\cdots$
[Ar V] λ7005	-0.43	0.1::	0.08::	0.3	0.1	0.7	0.3	17.0	3.7	$\cdots$	$\cdots$
He I λ7065	-0.44	7.4	5.7	14.0	5.2	9.3	4.6	20.0	4.2	21.0	10.1
[Ar III] λ7135	-0.45	16.0	12.2	37.0	13.4	58.0	28.1	161.0	32.4	55.0	26.1
[Ar IV] λ7170	-0.46	$\cdots$	$\cdots$	$\cdots$	$\cdots$	$\cdots$	$\cdots$	2.1::	0.4::	$\cdots$	$\cdots$
He II λ7178	-0.46	$\cdots$	$\cdots$	$\cdots$	$\cdots$	$\cdots$	$\cdots$	2.0::	0.4::	$\cdots$	$\cdots$
[Ar IV] λ7236	-0.47	$\cdots$	$\cdots$	0.6	0.2	$\cdots$	$\cdots$	1.6::	0.3::	0.5::	0.2::
[Ar IV] λ7264	-0.47	0.2	0.2	0.3	0.1	$\cdots$	$\cdots$	$\cdots$	$\cdots$	$\cdots$	$\cdots$
He I λ7281	-0.47	0.9::	0.7::	1.9::	0.7::	1.3::	0.6::	1.6::	0.3::	1.8:	0.8:
[O II] λ7323	-0.48	5.6	4.2	7.1	2.4	21.0	9.7	198.0	36.1	30.0	13.6
[Cl IV] λ7529	-0.51	0.7	0.5	0.9	0.3	$\cdots$	$\cdots$	2.6::	0.4::	0.4::	0.2::
He II λ7591	-0.52	$\cdots$	$\cdots$	0.9	0.3	$\cdots$	$\cdots$	$\cdots$	$\cdots$	$\cdots$	$\cdots$
[S I] λ7726	-0.54	$\cdots$	$\cdots$	$\cdots$	$\cdots$	$\cdots$	$\cdots$	$\cdots$	$\cdots$	$\cdots$	$\cdots$
[Ar III] λ7751	-0.54	4.0	2.9	9.9	3.0	15.0	6.4	50.0	7.3	14.0	5.8
[Cl IV] λ8045	-0.57	1.5:	1.1:	4.1:	1.1:	0.9:	0.4:	8.6	1.1	1.0:	0.4:
He II λ8236	-0.59	0.3::	0.2::	2.2::	0.6::	2.0::	0.8::	9.6	1.2	$\cdots$	$\cdots$
[Fe II] λ8446	-0.62	$\cdots$	$\cdots$	$\cdots$	$\cdots$	$\cdots$	$\cdots$	$\cdots$	$\cdots$	$\cdots$	$\cdots$
P17 λ8467	-0.62	0.5::	0.3::	0.9::	0.2::	$\cdots$	$\cdots$	$\cdots$	$\cdots$	1.4::	0.5::
P16 λ8502	-0.62	0.8::	0.6::	$\cdots$	$\cdots$	$\cdots$	$\cdots$	$\cdots$	$\cdots$	1.4	0.5
P15 λ8544	-0.63	1.0::	0.7::	1.4::	0.3::	$\cdots$	$\cdots$	8.1:	0.9:	1.7::	0.6:
P14 λ8598	-0.63	1.1::	0.8::	4.8::	1.2::	2.5::	0.9::	3.9::	0.4::	2.6::	0.9::
P13 λ8664	-0.64	1.7::	1.2::	3.2::	0.8::	1.5::	0.5::	10.0:	1.1:	2.9::	1.0::
P12 λ8750	-0.64	1.8::	1.2::	4.7:	1.1:	1.4::	0.5::	11.0:	1.1:	3.8:	1.3:
P11 λ8862	-0.65	2.3:	1.6:	8.3	1.9	6.5	2.3	13.0	1.3	4.7:	1.6:
P10 λ9014	-0.67	2.4:	1.6:	9.6	2.2	6.3	2.2	7.8	0.7	6.9	2.3
[S III] λ9069	-0.67	35.0	23.5	85.0	18.9	165	56.7	725	67.9	120	39.9
P9 λ9228	-0.68	4.3:	2.9:	11.0	2.4	7.2	2.4	32.0	2.9	10.0	3.3
[S III] λ9532	-0.70	53.0	35.0	241	50.3	228	74.7	1992	168	312	98.9
P8 λ9546	-0.70	6.7	4.4	23.0	4.8	7.9	2.6	77.0	6.5	16.0	5.1
c			0.26		0.97		0.69		1.54		0.71
log F$_{\mathrm{H}\beta}$[a]		-11.25		-12.13		-11.95		-12.56		-11.74	

[a]ergs cm^{-2} s^{-1} in our extracted spectra

Table 2B.   Line Strengths

Line	f(λ)	M1-80 F(λ)	M1-80 I(λ)	M3-15 F(λ)	M3-15 I(λ)	NGC 3587 F(λ)	NGC 3587 I(λ)	NGC 6309 F(λ)	NGC 6309 I(λ)	NGC 6439 F(λ)	NGC 6439 I(λ)
[O II] λ3727	0.29	131	223	⋯	⋯	272	272	11.0	17.0	23.7	43.0
He II + H10 λ3797	0.27	3.4	5.6	⋯	⋯	⋯	⋯	2.3	3.5	2.0::	3.5::
He II + H9 λ3835	0.26	3.8:	6.1:	⋯	⋯	⋯	⋯	3.4::	5.0::	3.6::	6.1::
[Ne III] λ3869	0.25	53.0	83.9	13.0	38.2	86.0	86.0	57.0	83.0	66.0	110
He I + H8 λ3889	0.25	12.0	18.8	⋯	⋯	21.0	21.0	9.5	13.7	11.0	18.2
Hε + [Ne III] λ3968	0.22	29.0	43.7	10.0	26.1	45.0	45.0	33.0	46.1	35.0	55.3
He I + He II λ4026	0.21	0.8::	1.2::	⋯	⋯	1.0::	1.0::	0.9::	1.2::	1.5:	2.3:
[S II] λ4072	0.20	2.3:	3.3:	⋯	⋯	⋯	⋯	2.0::	2.7::	3.1	4.6
He II + Hδ λ4101	0.19	19.0	26.8	7.2	16.1	29.0	29.0	22.0	29.1	18.0	26.4
He II λ4198	0.16	⋯	⋯	⋯	⋯	⋯	⋯	0.8	1.0	⋯	⋯
C II λ4267	0.14	0.6::	0.7::	⋯	⋯	⋯	⋯	⋯	⋯	⋯	⋯
Hγ λ4340	0.12	35.0	43.9	22.0	37.4	47.0	47.0	38.0	45.7	35.0	45.1
[O III] λ4363	0.12	5.9	7.3	1.5::	2.5::	7.6	7.6	9.9	11.8	6.4	8.1
He I λ4471	0.09	2.6	3.1	3.9:	5.7:	4.6	4.6	1.0	1.1	4.0	4.8
He II λ4540	0.07	0.8	0.9	⋯	⋯	⋯	⋯	2.6	2.9	0.2::	0.2::
N III λ4640	0.05	2.0	2.2	4.2::	5.1::	⋯	⋯	4.6	4.9	6.4	7.1
He II λ4686	0.04	34.0	36.3	⋯	⋯	14.0	14.0	81.0	85.5	20.0	21.5
He I + [Ar IV] λ4711	0.03	2.5	2.6	⋯	⋯	⋯	⋯	9.6	10.0	4.5	4.8
[Ne IV] λ4724	0.03	⋯	⋯	⋯	⋯	⋯	⋯	0.5::	0.5::	⋯	⋯
[Ar IV] λ4740	0.02	1.4	1.5	⋯	⋯	0.7::	0.7::	7.7	8.0	5.1	5.3
Hβ λ4861	0.00	100	100	100	100	100.0	100	100	100	100	100
He I λ4922	-0.02	⋯	⋯	1.5::	1.4::	⋯	⋯	⋯	⋯	⋯	⋯
[O III] λ4959	-0.03	412	390	333	293	298	298	364	348	437	411
[O III] λ5007	-0.04	1275	1182	1068	894	880	880	1106	1040	1359	1248
[N I] λ5199	-0.09	1.5::	1.3::	⋯	⋯	⋯	⋯	⋯	⋯	⋯	⋯
He II λ5411	-0.13	3.8	3.0	⋯	⋯	1.0::	1.0::	8.6	7.1	2.6	2.0
[Cl III] λ5517	-0.16	0.3::	0.2::	0.4::	0.2::	1.1::	1.1::	0.7::	0.6::	1.0:	0.7:
[Cl III] λ5537	-0.16	0.1::	0.08::	1.6::	0.8::	⋯	⋯	0.7::	0.6::	1.8:	1.3:
[O I] λ5577	-0.17	⋯	⋯	⋯	⋯	⋯	⋯	⋯	⋯	⋯	⋯
[N II] λ5755	-0.21	5.5	3.8	2.5:	1.0:	2.1::	2.1::	0.4::	0.3::	3.4	2.2
C IV λ5806	-0.22	⋯	⋯	⋯	⋯	⋯	⋯	⋯	⋯	3.1	2.0
He I λ5876	-0.23	14.4	9.5	51.0	19.0	11.0	11.0	10.0	7.1	27.0	16.8
He II λ6005	-0.26	⋯	⋯	⋯	⋯	⋯	⋯	⋯	⋯	⋯	⋯
He II λ6038	-0.26	⋯	⋯	⋯	⋯	⋯	⋯	⋯	⋯	⋯	⋯
He II λ6074	-0.27	0.2::	0.1::	⋯	⋯	⋯	⋯	⋯	⋯	⋯	⋯
[Ca V] λ6087	-0.27	0.1::	0.1::	⋯	⋯	⋯	⋯	⋯	⋯	⋯	⋯
[K IV] λ6101	-0.28	⋯	⋯	⋯	⋯	⋯	⋯	0.8::	0.5::	⋯	⋯
He II λ6119	-0.28	⋯	⋯	⋯	⋯	⋯	⋯	0.2::	0.1::	⋯	⋯
He II λ6172	-0.29	⋯	⋯	⋯	⋯	⋯	⋯	⋯	⋯	⋯	⋯
He II λ6235	-0.30	⋯	⋯	⋯	⋯	⋯	⋯	0.1::	0.1::	⋯	⋯
[O I] λ6300	-0.31	11.0	6.2	12.0	3.1	⋯	⋯	2.4:	1.6:	8.0	4.2
[S III] λ6312	-0.32	4.3:	2.4:	7.0:	1.8:	1.6::	1.6::	2.7:	1.7:	5.7	3.0
Mg II λ6346	-0.32	⋯	⋯	⋯	⋯	⋯	⋯	⋯	⋯	⋯	⋯
[O I] λ6363	-0.32	2.2:	1.2:	4.6:	1.1:	⋯	⋯	1.0::	0.6::	2.8	1.4
He II λ6407	-0.33	⋯	⋯	⋯	⋯	⋯	⋯	0.4::	0.3::	⋯	⋯
[Ar IV] λ6436	-0.34	⋯	⋯	⋯	⋯	⋯	⋯	2.2	1.3	1.4::	0.7::
[N II] λ6548	-0.36	124	64.6	78.0	16.9	37.0	37.0	10.0	5.9	91.0	43.9

Table 2B—Continued

Line	f(λ)	M1-80 F(λ)	M1-80 I(λ)	M3-15 F(λ)	M3-15 I(λ)	NGC 3587 F(λ)	NGC 3587 I(λ)	NGC 6309 F(λ)	NGC 6309 I(λ)	NGC 6439 F(λ)	NGC 6439 I(λ)
Hα λ6563	-0.36	551	286	1331	286	262	262	489	286	596	286
[N II] λ6584	-0.36	368	190	219	46.3	123	123	29.0	16.9	270	129
He I λ6678	-0.38	5.6	2.8	23.0	4.5	1.9	1.9	3.8	2.2	9.1	4.2
[S II] λ6716	-0.39	26.0	12.9	15.0	2.9	21.0	21.0	2.8:	1.6:	15.0	6.8
[S II] λ6731	-0.39	29.0	14.3	26.0	4.9	16.0	16.0	4.6:	2.6:	26.0	11.8
He II λ6891	-0.42	⋯	⋯	⋯	⋯	⋯	⋯	1.0::	0.5::	0.2::	0.1::
[Ar V] λ7005	-0.43	0.6::	0.3::	⋯	⋯	⋯	⋯	5.0	2.6	1.2	0.5
He I λ7065	-0.44	5.6	2.5	41.0	6.2	1.8:	1.8:	3.3	1.7	13.0	5.3
[Ar III] λ7135	-0.45	26.0	11.4	115	16.6	13.0	13.0	27.0	13.7	70.0	28.0
[Ar IV] λ7170	-0.46	⋯	⋯	⋯	⋯	⋯	⋯	⋯	⋯	⋯	⋯
He II λ7178	-0.46	0.9::	0.4::	⋯	⋯	⋯	⋯	1.8:	0.9:	⋯	⋯
[Ar IV] λ7236	-0.47	⋯	⋯	1.4	0.2	⋯	⋯	0.7::	0.3::	1.1::	0.4::
[Ar IV] λ7264	-0.47	⋯	⋯	⋯	⋯	⋯	⋯	0.6::	0.3::	0.3::	0.1::
He I λ7281	-0.47	⋯	⋯	5.1	0.7	⋯	⋯	0.6::	0.3::	1.8	0.7
[O II] λ7323	-0.48	23.0	9.6	45.0	5.8	5.8	5.8	5.9	2.9	14.0	5.3
[Cl IV] λ7529	-0.51	0.3::	0.1::	⋯	⋯	⋯	⋯	2.4	1.1	0.9	0.3
He II λ7591	-0.52	1.4:	0.5:	⋯	⋯	⋯	⋯	2.6:	1.2:	1.0::	0.3::
[S I] λ7726	-0.54	⋯	⋯	⋯	⋯	⋯	⋯	⋯	⋯	⋯	⋯
[Ar III] λ7751	-0.54	7.2	2.7	⋯	⋯	3.9:	3.9:	6.9	3.1	19.0	6.3
[Cl IV] λ8045	-0.57	0.6::	0.2::	2.2:	0.2 :	⋯	⋯	4.9	2.1	2.5	0.8
He II λ8236	-0.59	1.6::	0.5::	⋯	⋯	⋯	⋯	5.3	2.2	1.3	0.4
[Fe II] λ8446	-0.62	⋯	⋯	⋯	⋯	⋯	⋯	⋯	⋯	⋯	⋯
P17 λ8467	-0.62	1.1::	0.4::	3.4:	0.2:	⋯	⋯	0.7::	0.3::	1.6::	0.5::
P16 λ8502	-0.62	1.6::	0.5::	4.2:	0.3:	⋯	⋯	0.9::	0.4::	1.7:	0.5:
P15 λ8544	-0.63	1.6::	0.5::	6.3	0.4:	⋯	⋯	1.3:	0.5:	1.9:	0.5:
P14 λ8598	-0.63	2.1:	0.7:	11.0	0.7	⋯	⋯	2.3:	0.9:	2.3:	0.6:
P13 λ8664	-0.64	3.6:	1.1:	9.3	0.6	⋯	⋯	2.5:	1.0:	2.9:	0.8:
P12 λ8750	-0.64	3.6:	1.1:	12.0	0.8	⋯	⋯	3.6	1.4	3.9	1.0
P11 λ8862	-0.65	5.8	1.8	25.0	1.5	⋯	⋯	5.3	2.0	5.3	1.4
P10 λ9014	-0.67	5.4	1.6	23.0	1.3	⋯	⋯	6.6	2.4	5.2	1.3
[S III] λ9069	-0.67	87.0	25.7	270	15.5	⋯	⋯	57.0	21.0	226	58
P9 λ9228	-0.68	12.0	3.5	37.0	2.0	1.7::	1.7::	8.3	3.0	11.0	2.7
[S III] λ9532	-0.70	74.0	20.7	1366	69.0	49.0	49.0	110	38.8	143	34.4
P8 λ9546	-0.70	13.0	3.6	67.0:	3.4:	2.4::	2.4::	8.8	3.1	12.0	2.9
c			0.79		1.86		0.00		0.65		0.89
log F$_{Hβ}$[a]		-12.26		-12.67		-11.92		-11.74		-11.78	

[a]ergs cm^{-2} s^{-1} in our extracted spectra

Table 2C.   Line Strengths

Line	f(λ)	NGC 6572		NGC 6790		NGC 6879		NGC 6884	
		F(λ)	I(λ)	F(λ)	I(λ)	F(λ)	I(λ)	F(λ)	I(λ)
[O II] λ3727	0.29	24.0	29.7	11.0	18.3	8.7	11.1	17.0	27.0
He II + H10 λ3797	0.27	4.0	4.9	3.1	5.0	2.9	3.6	2.8:	4.3:
He II + H9 λ3835	0.26	5.3	6.4	1.4:	2.2:	5.6	7.0	4.5	6.8
[Ne III] λ3869	0.25	77.0	92.6	73.0	113	64.0	78.8	75.0	112
He I + H8 λ3889	0.25	12.0	14.4	97.0	149	16.0	19.6	11.0	16.3
Hε + [Ne III] λ3968	0.22	38.0	32.2	33.0	53.4	34.0	40.9	36.0	51.4
He I + He II λ4026	0.21	2.2:	2.6:	1.9:	2.7:	1.8:	2.1:	1.4:	1.9:
[S II] λ4072	0.20	2.6	3.0	1.7:	2.4:	1.0:	1.2:	2.1::	2.9::
He II + Hδ λ4101	0.19	23.0	26.4	18.0	25.0	20.0	23.4	20.0	26.9
He II λ4198	0.16	⋯	⋯	0.1::	0.1::	⋯	⋯	⋯	⋯
C II λ4267	0.14	0.4::	0.4::	0.3::	0.4::	⋯	⋯	0.5::	0.7::
Hγ λ4340	0.12	41.0	44.9	36.0	44.7	41.0	45.4	36.0	43.8
[O III] λ4363	0.12	7.9	8.6	16.0	19.7	7.0	7.7	9.9	11.9
He I λ4471	0.09	5.3	5.7	5.0	5.9	4.7	5.1	4.0	4.6
He II λ4540	0.07	⋯	⋯	⋯	⋯	⋯	⋯	0.6::	0.6::
N III λ4640	0.05	1.6:	1.7:	1.3:	1.4:	3.0	3.1	5.0	5.4
He II λ4686	0.04	0.6:	0.6:	3.5	3.7	2.6	2.7	19.0	20.1
He I + [Ar IV] λ4711	0.03	1.9	1.9	1.8	1.9	3.1	3.2	4.6	4.8
[Ne IV] λ4724	0.03	⋯	⋯	⋯	⋯	⋯	⋯	0.9::	1.0::
[Ar IV] λ4740	0.02	2.4	2.4	2.8	2.9	2.1	2.1	5.5	5.7
Hβ λ4861	0.00	100	100	100	100	100	100	100	100
He I λ4922	-0.02	⋯	⋯	1.5:	1.4:	1.6:	1.6:	0.9::	0.9::
[O III] λ4959	-0.03	407	398	506	480	353	344	493.	470
[O III] λ5007	-0.04	1206	1170	1550	1442	1070	1034	1542	1444
[N I] λ5199	-0.09	0.5::	0.5::	⋯	⋯	⋯	⋯	0.4::	0.4::
He I λ5411	-0.13	0.1::	0.1::	0.4::	0.3::	0.01::	0.01::	2.0::	1.6::
[Cl III] λ5517	-0.16	0.3:	0.3:	0.2:	0.2:	0.37::	0.32::	0.7:	0.6:
[Cl III] λ5537	-0.16	0.7:	0.6:	0.3::	0.2::	0.48::	0.42::	1.2:	0.9:
[O I] λ5577	-0.17	0.1::	0.1::	⋯	⋯	⋯	⋯	⋯	⋯
[N II] λ5755	-0.21	2.9	2.5	1.7	1.2	⋯	⋯	1.4:	1.0:
C IV λ5806	-0.22	1.1::	0.9::	⋯	⋯	1.3::	1.1::	⋯	⋯
He I λ5876	-0.23	22.0	18.6	31.0	20.1	20.0	16.5	22.0	15.2
He II λ6005	-0.26	⋯	⋯	⋯	⋯	⋯	⋯	0.1::	0.1::
He II λ6038	-0.26	⋯	⋯	⋯	⋯	⋯	⋯	⋯	⋯
He II λ6074	-0.27	⋯	⋯	⋯	⋯	⋯	⋯	⋯	⋯
[Ca V] λ6087	-0.27	⋯	⋯	⋯	⋯	⋯	⋯	0.1:	0.1:
[K IV] λ6101	-0.28	.12:	.10:	0.2:	0.1:	⋯	⋯	0.4::	0.3::
He II λ6119	-0.28	⋯	⋯	⋯	⋯	⋯	⋯	⋯	⋯
He II λ6172	-0.29	⋯	⋯	⋯	⋯	⋯	⋯	⋯	⋯
He II λ6235	-0.30	⋯	⋯	⋯	⋯	⋯	⋯	⋯	⋯
[O I] λ6300	-0.31	7.9	6.3	9.9	5.7	0.8:	0.6:	4.3	2.6
[S III] λ6312	-0.32	1.6:	1.3:	2.3	1.3	0.9:	0.7:	2.5	1.5
Mg II λ6346	-0.32	⋯	⋯	⋯	⋯	⋯	⋯	⋯	⋯
[O I] λ6363	-0.32	2.6	2.1	3.1	1.8	0.2::	0.2::	1.5:	0.9:
He II λ6407	-0.33	⋯	⋯	⋯	⋯	⋯	⋯	⋯	⋯
[Ar IV] λ6436	-0.34	⋯	⋯	⋯	⋯	⋯	⋯	0.26::	0.15::
[N II] λ6548	-0.36	26.0	20.0	13.0	7.0	6.6	4.9	24.0	13.6

Table 2C—Continued

Line	f(λ)	NGC 6572		NGC 6790		NGC 6879		NGC 6884	
		F(λ)	I(λ)	F(λ)	I(λ)	F(λ)	I(λ)	F(λ)	I(λ)
Hα λ6563	-0.36	372	286	537	286	385	286	506	286
[N II] λ6584	-0.36	78.0	59.8	38.0	20.1	13.0	9.6	72.0	40.4
He I λ6678	-0.38	5.6	4.2	8.9	4.6	5.2	3.8	6.8	3.7
[S II] λ6716	-0.39	1.2	0.9	0.9	0.4	0.8:	0.6:	2.8	1.5
[S II] λ6731	-0.39	2.4	1.8	2.0	1.0	1.5:	1.1:	5.3	2.9
He II λ6891	-0.42	$\cdots$	$\cdots$	$\cdots$	$\cdots$	$\cdots$	$\cdots$	0.3::	0.1::
[Ar V] λ7005	-0.43	0.05::	0.04::	0.1::	0.1::	$\cdots$	$\cdots$	0.5:	0.2:
He I λ7065	-0.44	13.0	9.4	36.0	16.6	7.8	5.4	13.0	6.4
[Ar III] λ7135	-0.45	27.5	19.7	20.0	9.1	17.0	11.7	39.0	19.0
[Ar IV] λ7170	-0.46	$\cdots$	$\cdots$	0.20::	0.06::	$\cdots$	$\cdots$	0.4:	0.2::
He II λ7178	-0.46	$\cdots$	$\cdots$	$\cdots$	$\cdots$	$\cdots$	$\cdots$	0.5:	0.2::
[Ar IV] λ7236	-0.47	0.4:	0.3:	0.6::	0.2::	$\cdots$	$\cdots$	0.7:	0.3:
[Ar IV] λ7264	-0.47	$\cdots$	$\cdots$	$\cdots$	$\cdots$	$\cdots$	$\cdots$	0.04::	0.02::
He I λ7281	-0.47	$\cdots$	$\cdots$	2.8	1.2	1.0:	0.7:	1.5	0.7
[O II] λ7323	-0.48	$\cdots$	$\cdots$	31.0	13.4	3.6	2.4	11.0	5.1
[Cl IV] λ7529	-0.51	0.2	0.1	0.6:	0.2:	0.4::	0.3::	0.8:	0.4:
He II λ7591	-0.52	$\cdots$	$\cdots$	$\cdots$	$\cdots$	$\cdots$	$\cdots$	0.8:	0.3:
[S I] λ7726	-0.54	$\cdots$	$\cdots$	$\cdots$	$\cdots$	$\cdots$	$\cdots$	$\cdots$	$\cdots$
[Ar III] λ7751	-0.54	7.2	4.9	5.5	2.1	4.2	2.7	10.0	4.3
[Cl IV] λ8045	-0.57	0.4	0.3	1.6	0.6	1.1:	0.7:	2.1	0.8
He II λ8236	-0.59	$\cdots$	$\cdots$	0.2::	0.1::	$\cdots$	$\cdots$	1.2:	0.5:
[Fe II] λ8446	-0.62	$\cdots$	$\cdots$	3.8:	1.3:	$\cdots$	$\cdots$	$\cdots$	$\cdots$
P17 λ8467	-0.62	0.7:	0.4:	1.5:	0.5:	0.6::	0.4::	1.1::	0.4::
P16 λ8502	-0.62	0.9:	0.6:	1.9:	0.6:	0.7::	0.4::	1.2::	0.4::
P15 λ8544	-0.63	1.1:	0.7:	2.2	0.7	1.0:	0.6:	1.5:	0.6:
P14 λ8598	-0.63	1.4:	0.9:	2.7	0.9	1.2	0.7	1.8	0.7
P13 λ8664	-0.64	1.7	1.1	3.5	1.2	1.2	0.7	2.5	0.9
P12 λ8750	-0.64	2.3	1.4	4.2	1.4	1.6	0.9	3.3	1.2
P11 λ8862	-0.65	2.9	1.8	5.8	1.9	2.8	1.6	4.5	1.6
P10 λ9014	-0.67	4.2	2.6	6.1	1.9	3.5	2.0	6.2	2.2
[S III] λ9069	-0.67	23.0	14.1	39.0	12.1	20.0	11.5	75.0	26.0
P9 λ9228	-0.68	5.2	3.2	10.0	3.0	5.7	3.2	9.2	3.1
[S III] λ9532	-0.70	75.0	45.0	81.0	23.9	57.0	32.0	97.0	32.0
P8 λ9546	-0.70	6.1	3.7	13.0	3.8	6.5:	3.6:	5.9::	1.9::
c			0.32		0.76		0.36		0.69
log F$_{\mathrm{H}\beta}$[a]			-9.96		-10.96		-11.62		-11.19

[a]ergs cm^{-2} s^{-1} in our extracted spectra

Table 2D.   Line Strengths

Line	f(λ)	NGC 6886		NGC 6891		NGC 6894		NGC 7026		Pe1-18	
		F(λ)	I(λ)	F(λ)	I(λ)	F(λ)	I(λ)	F(λ)	I(λ)	F(λ)	I(λ)
[O II] λ3727	0.29	104	152	12.0	13.2	131	201	35.0	59.5	⋯	⋯
He II + H10 λ3797	0.27	3.1	4.4	2.5	2.7	⋯	⋯	2.6	4.3	⋯	⋯
He II + H9 λ3835	0.26	4.1	5.8	4.8	5.2	⋯	⋯	3.4	5.5	10.0	38.1
[Ne III] λ3869	0.25	98.0	136	51.0	55.4	53.8	77.8	56.0	88.5	22.0	79.8
He I + H8 λ3889	0.25	15.0	20.7	17.0	18.4	9.8	14.2	11.0	17.2	⋯	⋯
Hε + [Ne III] λ3968	0.22	44.0	59.0	29.0	31.2	37.3	51.6	30.0	45.1	⋯	⋯
He I + He II λ4026	0.21	1.6:	2.1:	2.1:	2.2:	⋯	⋯	1.8:	2.6:	⋯	⋯
[S II] λ4072	0.20	5.6	7.2	0.6::	0.7::	⋯	⋯	3.8	5.4	5.8::	15.8::
He II + Hδ λ4101	0.19	22.0	28.1	23.0	24.5	19.1	25.3	17.0	23.9	3.5::	9.2::
He II λ4198	0.16	0.4::	0.5::	⋯	⋯	⋯	⋯	⋯	⋯	⋯	⋯
C II λ4267	0.14	0.3::	0.3::	0.3::	0.4::	⋯	⋯	⋯	⋯	⋯	⋯
Hγ λ4340	0.12	38.0	44.7	44.0	45.8	35.7	42.6	34.0	42.6	23.0	43.4
[O III] λ4363	0.12	16.0	18.7	4.6	4.8	⋯	⋯	3.2:	4.0:	5.4	9.9
He I λ4471	0.09	3.3	3.7	5.0	5.2	5.0::	5.7::	4.9	5.8	⋯	⋯
He II λ4540	0.07	1.2::	1.3::	⋯	⋯	2.8::	3.1::	⋯	⋯	⋯	⋯
N III λ4640	0.05	3.8	4.0	2.3	2.3	⋯	⋯	4.2	4.6	⋯	⋯
He II λ4686	0.04	37.0	38.8	⋯	⋯	16.0	17.0	15.0	16.0	⋯	⋯
He I + [Ar IV] λ4711	0.03	6.2	6.4	1.3:	1.3:	⋯	⋯	2.5	2.6	⋯	⋯
[Ne IV] λ4724	0.03	1.1:	1.1:	0.1::	0.1::	⋯	⋯	⋯	⋯	⋯	⋯
[Ar IV] λ4740	0.02	6.7	6.9	0.7::	0.7::	⋯	⋯	2.9	3.0	⋯	⋯
Hβ λ4861	0.00	100	100	100	100	100	100	100	100	100	100
He I λ4922	-0.02	1.0:	1.0:	1.5:	1.5:	⋯	⋯	1.5:	1.4:	⋯	⋯
[O III] λ4959	-0.03	516	496	295	292	254	243	336	318	478	410
[O III] λ5007	-0.04	1549	1467	889	877	769	725	1051	975	1512	1222
[N I] λ5199	-0.09	2.4	2.1	⋯	⋯	⋯	⋯	1.4:	1.2:	⋯	⋯
He II λ5411	-0.13	4.0	3.4	⋯	⋯	1.9:	1.6:	1.8::	1.4::	⋯	⋯
[Cl III] λ5517	-0.16	0.9::	0.7::	0.3:	0.3:	⋯	⋯	1.2:	0.9:	1.0:	0.44:
[Cl III] λ5537	-0.16	1.7:	1.4:	0.4:	0.4:	⋯	⋯	1.6:	1.2:	2.1:	0.93:
[O I] λ5577	-0.17	0.3::	0.2::	⋯	⋯	⋯	⋯	⋯	⋯	⋯	⋯
[N II] λ5755	-0.21	8.4	6.4	⋯	⋯	5.1	3.7	3.5	2.4	11.8:	4.0:
C IV λ5806	-0.22	⋯	⋯	1.5	1.4	⋯	⋯	⋯	⋯	⋯	⋯
He I λ5876	-0.23	18.0	13.3	17.0	15.8	21.1	15.0	27.0	17.7	74.0	22.7
He II λ6005	-0.26	⋯	⋯	⋯	⋯	⋯	⋯	⋯	⋯	⋯	⋯
He II λ6038	-0.26	⋯	⋯	⋯	⋯	⋯	⋯	⋯	⋯	⋯	⋯
He II λ6074	-0.27	⋯	⋯	⋯	⋯	⋯	⋯	⋯	⋯	⋯	⋯
[Ca V] λ6087	-0.27	0.1	0.1	⋯	⋯	⋯	⋯	⋯	⋯	⋯	⋯
[K IV] λ6101	-0.28	0.3::	0.2::	⋯	⋯	⋯	⋯	0.5::	0.3::	⋯	⋯
He II λ6119	-0.28	⋯	⋯	⋯	⋯	⋯	⋯	0.2::	0.1::	⋯	⋯
He II λ6172	-0.29	⋯	⋯	⋯	⋯	⋯	⋯	⋯	⋯	⋯	⋯
He II λ6235	-0.30	0.3::	0.2::	⋯	⋯	⋯	⋯	⋯	⋯	⋯	⋯
[O I] λ6300	-0.31	26.0	17.3	⋯	⋯	14.4:	9.1:	10.0	5.7	29.0	5.9
[S III] λ6312	-0.32	5.5	3.6	0.5::	0.5::	5.4:	3.4:	5.0	2.8	18.0	3.6
Mg II λ6346	-0.32	⋯	⋯	⋯	⋯	⋯	⋯	⋯	⋯	⋯	⋯
[O I] λ6363	-0.32	8.8	5.8	⋯	⋯	4.1:	2.6:	3.6	2.0	7.5	1.4
He II λ6407	-0.33	0.3::	0.2::	⋯	⋯	⋯	⋯	⋯	⋯	⋯	⋯
[Ar IV] λ6436	-0.34	1.5:	1.0:	⋯	⋯	⋯	⋯	⋯	⋯	⋯	⋯
[N II] λ6548	-0.36	134	83.9	2.7	2.4	182	107	91.0	47.5	242	38.9

Table 2D—Continued

Line	f(λ)	NGC 6886		NGC 6891		NGC 6894		NGC 7026		Pe1-18	
		F(λ)	I(λ)	F(λ)	I(λ)	F(λ)	I(λ)	F(λ)	I(λ)	F(λ)	I(λ)
Hα λ6563	-0.36	458	286	322	286	488	287	550	286	1800	286
[N II] λ6584	-0.36	404	251	6.1:	5.4:	559	329	279	144	713	111
He I λ6678	-0.38	5.4	3.3	4.5	4.0	6.5	3.7	8.5	4.3	32.0	4.6
[S II] λ6716	-0.39	12.0	7.2	⋯	⋯	86.4	48.6	18.0	8.9	15.0	2.1
[S II] λ6731	-0.39	23.0	13.8	0.3	0.3	73.9	41.6	30.0	14.8	35.0	4.8
He II λ6891	-0.42	0.4:	0.3:	⋯	⋯	⋯	⋯	0.3:	0.1:	⋯	⋯
[Ar V] λ7005	-0.43	3.1	1.8	⋯	⋯	⋯	⋯	⋯	⋯	⋯	⋯
He I λ7065	-0.44	10.0	5.6	5.7	4.9	4.9:	2.6:	11.0	4.9	115	12.0
[Ar III] λ7135	-0.45	52.0	28.7	15.0	12.9	48.9	25.2	58.0	25.5	351	34.6
[Ar IV] λ7170	-0.46	1.0::	0.5::	⋯	⋯	⋯	⋯	⋯	⋯	⋯	⋯
He II λ7178	-0.46	⋯	⋯	⋯	⋯	⋯	⋯	⋯	⋯	⋯	⋯
[Ar IV] λ7236	-0.47	0.5::	0.3::	0.4::	0.3::	⋯	⋯	0.8::	0.3::	4.3::	0.4::
[Ar IV] λ7264	-0.47	0.3::	0.2::	⋯	⋯	⋯	⋯	⋯	⋯	⋯	⋯
He I λ7281	-0.47	1.1::	0.6::	0.9:	0.8:	⋯	⋯	1.4::	0.6::	10.7	1.0
[O II] λ7323	-0.48	45.0	24.0	2.0:	1.7:	15.4	7.6	13.0	5.4	134	114
[Cl IV] λ7529	-0.51	0.6::	0.3::	⋯	⋯	⋯	⋯	0.8::	0.3::	0.9::	0.1::
He II λ7591	-0.52	1.4:	0.7:	⋯	⋯	⋯	⋯	⋯	⋯	⋯	⋯
[S I] λ7726	-0.54	0.1::	0.1::	⋯	⋯	⋯	⋯	⋯	⋯	⋯	⋯
[Ar III] λ7751	-0.54	14.0	6.9	3.8	3.2	12.7	5.7	17.0	6.4	113.0	7.2
[Cl IV] λ8045	-0.57	2.1	1.0	0.09:	0.07:	⋯	⋯	1.8:	0.6:	11.0	0.6
He II λ8236	-0.59	1.9:	0.9:	⋯	⋯	⋯	⋯	1.2::	0.4::	⋯	⋯
[Fe II] λ8446	-0.62	⋯	⋯	⋯	⋯	⋯	⋯	⋯	⋯	14.0	0.6
P17 λ8467	-0.62	0.7::	0.3::	0.6::	0.5::	⋯	⋯	1.4::	0.5::	13.0:	0.6:
P16 λ8502	-0.62	0.9::	0.4::	0.6::	0.5::	⋯	⋯	1.6:	0.5:	8.9	0.4
P15 λ8544	-0.63	1.5:	0.7:	0.8:	0.6:	⋯	⋯	1.6:	0.5:	11.0	0.4
P14 λ8598	-0.63	1.6:	0.7:	1.1:	0.9:	⋯	⋯	2.0:	0.6:	26.0	1.0
P13 λ8664	-0.64	2.5	1.1	1.4:	1.1:	⋯	⋯	2.9	0.9	22.0	0.8
P12 λ8750	-0.64	3.0	1.3	1.8:	1.5:	⋯	⋯	3.5	1.1	30.0	1.1
P11 λ8862	-0.65	3.6	1.5	2.2	1.8	6.1	2.3	5.4	1.6	48.0	1.7
P10 λ9014	-0.67	4.9	2.1	2.5	2.0	5.5	2.0	6.5	1.9	54.0	1.8
[S III] λ9069	-0.67	100	41.7	8.2	6.6	143.0	53.3	207	61.3	880	28.7
P9 λ9228	-0.68	7.6	3.1	3.8	3.0	6.4	2.3	10.0	2.9	82.0	2.5
[S III] λ9532	-0.70	124	49.7	19.0	15.1	157.0	56.0	399	112	2848	80.1
P8 λ9546	-0.70	5.8	2.3	4.9	3.9	14.4	5.1	9.8	2.7	92.0	2.6
c			0.57		0.14		0.64		0.79		2.22
log F$_{H\beta}$[a]		-11.41		-10.97		-12.38		-11.25		-12.99	

[a]ergs cm^{-2} s^{-1} in our extracted spectra

Table 3A.   Extinction Quantity c

Object	c(Hα)	c(P10)	c(P8)
IC 5217	0.26	0.17	0.38
M1-50	0.97	1.07	1.14
M1-54	0.69	0.80	0.48
M1-57	1.54	.94	1.89
M1-74	0.71	0.86	0.92
M1-80	0.79	0.70	0.79
M3-15	1.86	1.64	1.80
NGC 3587	$\cdots$	$\cdots$	$\cdots$
NGC 6309	0.65	0.83	0.55
NGC 6439	0.89	0.67	0.74
NGC 6572	0.32	0.53	0.32
NGC 6790	0.76	0.78	0.79
NGC 6879	0.36	0.42	0.36
NGC 6884	0.69	0.79	0.30
NGC 6886	0.57	0.63	0.29
NGC 6891	0.14	0.20	0.18
NGC 6894	0.64	0.71	0.85
NGC 7026	0.79	0.82	0.61
Pe1-18	2.22	2.19	2.00

Table 3B.   Line Ratios[a]

Object	[Ne III]	[O III]	[N II]	[Ar III]	P10/Hβ	P8/Hβ	[S III]
IC 5217	2.28	3.02	2.81	4.21	0.016	0.044	1.49
M1-50	2.40	3.04	2.74	4.47	0.022	0.048	2.66
M1-54	2.35	2.99	3.10	4.39	0.022	0.026	1.32
M1-57	2.66	3.08	3.01	$\cdots$	0.007	0.065	2.48
M1-74	1.89	3.04	3.02	4.50	0.023	0.051	2.48
M1-80	1.92	3.03	2.93	4.22	0.016	0.036	0.81
M3-15	1.46	3.06	2.74	$\cdots$	0.013	0.034	4.45
NGC 3587	1.91	2.95	3.32	3.33	$\cdots$	0.024	$\cdots$
NGC 6309	1.80	2.99	2.86	4.42	0.024	0.031	1.85
NGC 6439	2.00	3.04	2.93	4.43	0.013	0.029	0.60
NGC 6572	2.07	2.94	2.99	$\cdots$	0.026	0.037	3.19
NGC 6790	2.32	3.00	2.87	4.33	0.019	0.038	1.89
NGC 6879	1.88	3.00	1.96	4.33	0.020	0.036	2.78
NGC 6884	2.18	3.07	2.97	4.42	0.022	0.019	1.23
NGC 6886	2.31	2.96	2.99	4.16	0.021	0.023	1.19
NGC 6891	1.78	3.00	2.25	4.03	0.020	0.039	2.29
NGC 6894	1.51	2.98	3.07	4.42	0.020	0.051	1.05
NGC 7026	1.96	3.06	3.03	3.98	0.019	0.027	1.83
Pe1-18	$\cdots$	2.98	2.85	4.81	0.018	0.026	2.79
Mean	2.04$\pm$.30	3.01$\pm$.04	2.87$\pm$.30	4.28$\pm$.32	0.019$\pm$.004	0.036$\pm$.01	2.02$\pm$.94
Theory	3.32	2.89	2.95	4.14	0.018	0.037	2.48

[a][Ne III]: $\lambda3869/\lambda3968$; [O III]: $\lambda5007/\lambda4959$; [N II]: $\lambda6584/\lambda6548$; [Ar III]: $\lambda7135/\lambda7751$; P10/Hβ: $\lambda9014/\lambda4861$; P8/Hβ: $\lambda9546/\lambda4861$; [S III]: $\lambda9532/\lambda9069$.

Table 4.   ABUN: Sources Of Atomic Data

Ion	Emission Line (Å)	Data Type[a]	Reference[b]
H^0	4861	$\alpha_{\mathrm{eff}}(\lambda 4861)$	1
He^0	5876	$\alpha_{\mathrm{eff}}(\lambda 5876)^c$	2
He^+	4686	$\alpha_{\mathrm{eff}}(\lambda 4686)$	1
O^o	6300	Ω	3
		A	4
O^+	3727, 7323	Ω	5 (2-3,4-5 only), 6 (all other transitions)
		A	4
O^{+2}	4363, 5007	Ω	7 (4-5 only); 8 (all other transitions)
		A	4
N^+	5755, 6584	Ω	8
		A	4
Ne^{+2}	3869	Ω	9
		A	10
S^+	4072, 6716, 6731	Ω	11
		A	5
S^{+2}	6312, 9069, 9532	Ω	12
		A	5
Cl^{+2}	5537	Ω	13
		A	5
Cl^{+3}	8045	Ω	12
		A	5
Ar^{+2}	7135	Ω	12
		A	14
Ar^{+3}	4740	Ω	15
		A	16

[a]α_{eff}=effective recombination coefficient; Ω=collision strength; A=transition rate.

[b]References.–(1) Storey & Hummer 1995; (2) Péquignot et al. 1991; (3) Bhatia & Kastner 1995; (4) Wiese, Fuhr, & Deters 1996; (5) Mendoza 1983; (6) McLaughlin & Bell 1993; (7) Burke, Lennon, & Seaton 1989; (8) Lennon & Burke 1994; (9) Butler & Zeippen 1994; (10) Baluja & Zeippen 1988; (11) Ramsbottom, Bell, & Stafford 1996; (12) Galavís et al. 1995; (13) Butler & Zeippen 1989; (14) Mendoza & Zeippen 1983; (15) Zeippen, Le Bourlot, & Butler 1987; (16) Mendoza & Zeippen 1982.

[c]Includes collisional effects given by Clegg (1987).

Table 5A.   Ionic Abundances, Temperatures, & Densities[a]

Parameter	IC 5217	M1-50	M1-54	M1-57	M1-74
He^+/H^+	9.88E-02	9.46E-02	0.14	8.46E-02	0.12
He^{+2}/H^+	8.76E-03	2.19E-02	1.73E-02	1.89E-03	$\cdots$
ICF(He)	1.00	1.00	1.00	1.00	1.00
O^o/H^+	2.04E-06	5.61E-07	6.87E-05	4.14E-05	3.96E-06
O^+/H^+	8.88E-06	1.35E-05	1.68E-04	4.86E-05	5.19E-06
O^{+2}/H^+	3.33E-04	4.84E-04	3.22E-04	3.71E-04	4.69E-04
ICF(O)	1.09	1.23	1.12	1.02	1.00
N^+/H^+	3.68E-06	1.73E-06	1.96E-04	6.58E-05	4.73E-06
ICF(N)	41.93	45.27	3.27	8.84	91.40
Ne^{+2}/H^+	7.78E-05	9.44E-05	1.20E-04	6.98E-05	1.19E-04
ICF(Ne)	1.12	1.27	1.71	1.16	1.01
S^+/H^+	1.63E-07	8.52E-08	3.55E-06	2.17E-06	1.26E-07
S^{+2}/H^+_{NIR}	2.60E-06	2.22E-06	7.73E-06	5.43E-06	5.04E-06
S^{+2}/H^+_{6312}	1.81E-06	3.08E-06	1.38E-05	1.23E-05	2.60E-06
ICF(S)	1.91	1.96	1.13	1.29	2.74
Cl^{+2}/H^+	5.27E-08[b]	6.71E-08[c]	1.65E-07[b]	1.24E-07[b]	6.77E-08[c]
Cl^{+3}/H^+	7.01E-08[b]	8.43E-08[b]	3.02E-08[b]	6.32E-08	3.82E-08[b]
ICF(Cl)	1.09	1.23	1.12	1.02	1.00
Ar^{+2}/H^+	9.26E-07	1.13E-06	2.70E-06	2.05E-06	2.89E-06
Ar^{+3}/H^+	5.89E-07	8.52E-07	4.75E-07	8.70E-07	3.28E-07
ICF(Ar)	1.12	1.26	$\cdots$	1.15	1.01
$T_{O3}(K)$	11000	10400	9900	11900	9300
$T_{N2}(K)$	12600.	10600	8600	11200	14700
$T_{O2}(K)$	12300	$\cdots$	6500	16000	(33400)
$T_{S2}(K)$	8800	$\cdots$	10400	5800	$\cdots$
$T_{S3}(K)$	11200	11900	10100	15800	11400
$N_{e,S2}(cm^{-3})$	10000	4400	1500	4500	2100

[a]Unless otherwise noted, uncertainties in ionic abundances, electron temperatures, and electron densities are $\pm30\%$, $\pm10\%$, and $\pm10\%$, respectively.

[b]Uncertainty is estimated to be $\pm50\%$

[c]Uncertainty is estimated to be $\pm75\%$

Table 5B. Ionic Abundances, Temperatures, & Densities[a]

Parameter	M1-80	M3-15	NGC 3587	NGC 6309	NGC 6439
He^+/H^+	0.07	0.13	8.52E-02	4.81E-02	0.12
He^{+2}/H^+	3.27E-02	0.	1.29E-02	7.90E-02	1.95E-02
$ICF(He)$	1.00	1.00	1.00	1.00	1.00
O^o/H^+	1.25E-05	6.67E-06	$\cdots$	3.12E-06	9.93E-06
O^+/H^+	1.00E-04	4.61E-05	1.21E-04	1.05E-05	3.37E-05
O^{+2}/H^+	4.99E-04	7.91E-04	2.72E-04	2.37E-04	4.98E-04
$ICF(O)$	1.47	1.00	1.15	2.64	1.17
N^+/H^+	3.93E-05	1.08E-05	2.61E-05	3.32E-06	3.03E-05
$ICF(N)$	8.78	18.14	3.73	62.19	18.35
Ne^{+2}/H^+	1.06E-04	1.24E-04	7.22E-05	4.90E-05	1.31E-04
$ICF(Ne)$	1.76	1.06	1.66	2.76	1.24
S^+/H^+	7.52E-07	3.38E-07	9.21E-07	1.51E-07	8.43E-07
S^{+2}/H^+_{NIR}	2.79E-06	4.05E-06	2.14E-06	2.04E-06	8.00E-06
S^{+2}/H^+_{6312}	6.43E-06[b]	4.80E-06[b]	4.98E-06[c]	4.27E-06[b]	9.14E-06
$ICF(S)$	1.29	1.48	1.15	2.25	1.49
Cl^{+2}/H^+	1.33E-08[c]	2.30E-07[c]	$\cdots$	4.68E-08[c]	1.80E-07[b]
Cl^{+3}/H^+	2.04E-08[c]	2.92E-08[b]	$\cdots$	1.24E-07	6.84E-08
$ICF(Cl)$	1.47	1.00	1.15	2.64	1.17
Ar^{+2}/H^+	1.19E-06	2.94E-06	1.07E-06	9.19E-07	5.98E-07
Ar^{+3}/H^+	3.50E-07	$\cdots$	1.30E-07[c]	9.98E-07	1.08E-06
$ICF(Ar)$	1.66	1.06	$\cdots$	2.69	1.23
$T_{O3}(K)$	9500	7800	10600	11600	9700
$T_{N2}(K)$	10000	10400	9400	9600	9500
$T_{O2}(K)$	6200	$\cdots$	11600	10800	9000
$T_{S2}(K)$	10400	$\cdots$	$\cdots$	14200	6700
$T_{S3}(K)$	13500	11100	12400	12300	10000
$N_{e,S2}(cm^{-3})$	800	3600	100	3600	4100

[a]Unless otherwise noted, uncertainties in ionic abundances, electron temperatures, and electron densities are $\pm30\%$, $\pm10\%$, and $\pm10\%$, respectively.

[b]Uncertainty is estimated to be $\pm50\%$

[c]Uncertainty is estimated to be $\pm75\%$

Table 5C. Ionic Abundances, Temperatures, & Densities[a]

Parameter	NGC 6572	NGC 6790	NGC 6879	NGC 6884
He^+/H^+	0.13	0.12	0.11	0.10
He^{+2}/H^+	5.52E-04[b]	3.43E-03	2.44E-03	1.84E-02
ICF(He)	1.00	1.00	1.00	1.00
O^o/H^+	5.05E-06	2.64E-06	1.11E-06[b]	3.79E-06
O^+/H^+	9.62E-06	1.90E-05	8.17E-06	1.43E-05
O^{+2}/H^+	4.17E-04	3.07E-04	3.63E-04	4.57E-04
ICF(O)	1.00	1.03	1.02	1.18
N^+/H^+	7.96E-06	3.37E-06	1.99E-06	7.14E-06
ICF(N)	44.53	17.17	46.40	38.89
Ne^{+2}/H^+	9.43E-05	5.22E-05	7.90E-05	9.88E-05
ICF(Ne)	1.03	1.06	1.04	1.21
S^+/H^+	1.04E-07	2.60E-07	8.39E-08	1.80E-07
S^{+2}/H^+_{NIR}	2.12E-06	1.09E-06	1.66E-06	3.20E-06
S^{+2}/H^+_{6312}	1.13E-06[b]	5.66E-07	1.62E-06[b]	2.61E-06
ICF(S)	1.95	1.46	1.98	1.85
Cl^{+2}/H^+	7.53E-08[b]	3.04E-08[c]	$\cdots$	1.02E-07[b]
Cl^{+3}/H^+	2.30E-08	2.93E-08	5.43E-08[b]	6.26E-08
ICF(Cl)	1.00	1.00	1.02	1.18
Ar^{+2}/H^+	1.82E-06	5.21E-07	1.07E-06	1.61E-06
Ar^{+3}/H^+	3.97E-07	2.67E-07	3.56E-07	8.83E-07
ICF(Ar)	1.03	1.06	1.04	1.21
$T_{O3}(K)$	10100	12400	10100	10400
$T_{N2}(K)$	14500	18300	10300	11100
$T_{O2}(K)$	$\cdots$	(94000)	12700	11600
$T_{S2}(K)$	(38200)	$\cdots$	15800	14400
$T_{S3}(K)$	11500	14800	10400	10500
$N_{e,S2}(cm^{-3})$	9500	>10000	7400	6500

[a]Unless otherwise noted, uncertainties in ionic abundances, electron temperatures, and electron densities are ±30%, ±10%, and ±10%, respectively.

[b]Uncertainty is estimated to be ±50%

[c]Uncertainty is estimated to be ±75%

Table 5D.   Ionic Abundances, Temperatures, & Densities[a]

Parameter	NGC 6886	NGC 6891	NGC 7026	Pe1-18
He^+/H^+	8.47E-02	0.11	0.12	0.15
He^{+2}/H^+	3.58E-02	$\cdots$	1.40E-02	$\cdots$
ICF(He)	1.00	1.00	1.00	1.00
O^o/H^+	2.11E-05	$\cdots$	1.53E-05	5.88E-06
O^+/H^+	7.12E-05	7.14E-06	5.03E-05	1.41E-04
O^{+2}/H^+	2.97E-04	4.17E-04	6.06E-04	4.54E-04
ICF(O)	1.42	1.00	1.11	1.00
N^+/H^+	.83E-05	9.49E-07[b]	3.80E-05	3.14E-05
ICF(N)	7.36	59.48	14.54	4.23
Ne^{+2}/H^+	6.92E-05	8.11E-05	1.84E-04	7.19E-05
ICF(Ne)	1.76	1.02	1.21	1.31
S^+/H^+	7.85E-07	1.66E-08	1.12E-06	1.91E-06
S^{+2}/H^+_{NIR}	3.72E-06	8.72E-07	9.95E-06	3.43E-06
S^{+2}/H^+_{6312}	5.26E-06	6.48E-07[c]	1.00E-05	3.32E-06
ICF(S)	1.26	2.20	1.41	1.17
Cl^{+2}/H^+	1.01E-07[c]	6.09E-08[b]	2.53E-07[b]	1.96E-07
Cl^{+3}/H^+	5.30E-08	6.79E-09	7.68E-08	4.31E-08
ICF(Cl)	1.42	1.00	1.11	1.00
Ar^{+2}/H^+	1.75E-06	1.46E-06	3.52E-06	2.97E-06
Ar^{+3}/H^+	7.16E-07	1.48E-07[c]	9.32E-07	$\cdots$
ICF(Ar)	1.65	1.02	1.20	1.31
$T_{O3}(K)$	12100	9200	8500	10300
$T_{N2}(K)$	11200	12300	9400	13300
$T_{O2}(K)$	10300	9200	7800	$\cdots$
$T_{S2}(K)$	8200	$\cdots$	6400	$\cdots$
$T_{S3}(K)$	12900	11500	9500	15000
$N_{e,S2}(cm^{-3})$	7200	10000	3300	>10000

[a]Unless otherwise noted, uncertainties in ionic abundances, electron temperatures, and electron densities are $\pm30\%$, $\pm10\%$, and $\pm10\%$, respectively.

[b]Uncertainty is estimated to be $\pm50\%$

[c]Uncertainty is estimated to be $\pm75\%$

Table 6A.   Elemental Abundances[a]

Element	IC 5217	M1-50	M1-54	M1-57	M1-74	Sun[b]	Orion[c]
He/H	0.11	0.12	0.16	0.09	0.12	0.10	0.10
O/H ($\times 10^4$)	3.72	6.12	5.51	4.29	4.74	7.41	5.25
N/H ($\times 10^4$)	1.54	0.78	6.40	5.82	4.33	0.93	0.60
Ne/H ($\times 10^4$)	0.87	1.19	2.06	0.81	1.20	1.20	0.78
S/H ($\times 10^5$)	0.53	0.45	1.28	0.98	1.41	2.14	1.48
Cl/H ($\times 10^7$)	1.34	1.86	2.20	1.91	1.06	3.16	2.14
Ar/H ($\times 10^6$)	1.69	2.50	2.70[d]	3.37	3.26	3.31	3.09
N/O	0.41	0.13	1.16	1.35	0.91	0.13	0.11
Ne/O	0.23	0.20	0.37	0.19	0.25	0.16	0.15
S/O ($\times 10^1$)	0.14	0.07	0.23	0.23	0.30	0.29	0.28
Cl/O ($\times 10^3$)	0.36	0.30	0.40	0.45	0.22	0.43	0.41
Ar/O ($\times 10^2$)	0.45	0.41	0.49[d]	0.78	0.69	0.45	0.59

[a]Uncertainties in elemental abundances are generally as follows.   S/O: $\pm 30\%$; Cl/O: $\pm 50\%$; Ar/O: $\pm 75\%$.

[b]Grevesse et al. (1996)

[c]Esteban et al. (1998), Table 19, gas + dust

[d]$Ar = Ar^{+2}$

Table 6B.   Elemental Abundances[a]

Element	M1-80	M3-15	NGC 3587	NGC 6309	NGC 6439	Sun[b]	Orion[c]
He/H	0.10	0.13	0.10	0.13	0.14	0.10	0.10
O/H ($\times 10^4$)	8.79	8.37	4.53	6.55	6.19	7.41	5.25
N/H ($\times 10^4$)	3.45	1.97	0.97	2.06	5.56	0.93	0.60
Ne/H ($\times 10^4$)	1.87	1.31	1.20	1.35	1.62	1.20	0.78
S/H ($\times 10^5$)	0.46	0.65	0.35	0.49	1.31	2.14	1.48
Cl/H ($\times 10^7$)	0.50	2.60	$\cdots$	4.50	2.90	3.16	2.14
Ar/H ($\times 10^6$)	2.55	3.12	1.07[d]	5.15	2.06	3.31	3.09
N/O	0.39	0.23	0.21	0.32	0.90	0.13	0.11
Ne/O	0.21	0.16	0.27	0.21	0.26	0.16	0.15
S/O ($\times 10^1$)	0.05	0.08	0.08	0.08	0.21	0.29	0.28
Cl/O ($\times 10^3$)	0.06	0.31	$\cdots$	0.69	0.47	0.43	0.41
Ar/O ($\times 10^2$)	0.29	0.37	0.24[d]	0.79	0.33	0.45	0.59

[a]Uncertainties in elemental abundances are generally as follows. S/O: $\pm 30\%$; Cl/O: $\pm 50\%$; Ar/O: $\pm 75\%$.

[b]Grevesse et al. (1996)

[c]Esteban et al. (1998), Table 19, gas + dust

[d]Ar=Ar^{+2}

–

Table 6C.   Elemental Abundances[a]

Element	NGC 6572	NGC 6790	NGC 6879	NGC 6884	Sun[b]	Orion[c]
He/H	0.13	0.12	0.11	0.12	0.10	0.10
O/H ($\times 10^4$)	4.29	3.36	3.79	5.55	7.41	5.25
N/H ($\times 10^4$)	3.54	0.60	0.92	2.78	0.93	0.60
Ne/H ($\times 10^4$)	0.97	0.57	0.83	1.20	1.20	0.78
S/H ($\times 10^5$)	0.43	0.20	0.34	0.63	2.14	1.48
Cl/H ($\times 10^7$)	0.99	0.61	0.55	1.94	3.16	2.14
Ar/H ($\times 10^6$)	2.27	0.86	1.49	3.02	3.31	3.09
N/O	0.83	0.18	0.24	0.50	0.13	0.11
Ne/O	0.23	0.17	0.22	0.22	0.16	0.15
S/O ($\times 10^1$)	0.10	0.06	0.09	0.11	0.29	0.28
Cl/O ($\times 10^3$)	0.23	0.18	0.15	0.35	0.43	0.41
Ar/O ($\times 10^2$)	0.53	0.26	0.39	0.54	0.45	0.59

[a]Uncertainties in elemental abundances are generally as follows. S/O: $\pm 30\%$; Cl/O: $\pm 50\%$; Ar/O: $\pm 75\%$.

[b]Grevesse et al. (1996)

[c]Esteban et al. (1998), Table 19, gas + dust

Table 6D.   Elemental Abundances[a]

Element	NGC 6886	NGC 6891	NGC 7026	Pe1-18	Sun[b]	Orion[c]
He/H	0.12	0.11	0.14	0.15	0.10	0.10
O/H ($\times 10^4$)	5.24	4.25	7.31	5.95	7.41	5.25
N/H ($\times 10^4$)	2.82	0.56	5.52	1.33	0.93	0.60
Ne/H ($\times 10^4$)	1.22	0.83	2.22	0.94	1.20	0.78
S/H ($\times 10^5$)	0.57	0.18	1.56	0.62	2.14	1.48
Cl/H ($\times 10^7$)	2.19	0.68	3.67	2.39	3.16	2.14
Ar/H ($\times 10^6$)	4.06	1.64	5.32	3.89	3.31	3.09
N/O	0.54	0.13	0.76	0.22	0.13	0.11
Ne/O	0.23	0.19	0.30	0.16	0.16	0.15
S/O ($\times 10^1$)	0.11	0.04	0.21	0.10	0.29	0.28
Cl/O ($\times 10^3$)	0.42	0.16	0.50	0.40	0.43	0.41
Ar/O ($\times 10^2$)	0.78	0.39	0.73	0.65	0.45	0.59

[a]Uncertainties in elemental abundances are generally as follows. S/O: $\pm 30\%$; Cl/O: $\pm 50\%$; Ar/O: $\pm 75\%$.

[b]Grevesse et al. (1996)

[c]Esteban et al. (1998), Table 19, gas + dust

Table 7.   Comparison of Abundance Averages

Ratio	This Paper	KB[1]	AK[2]	Sun[3]	Orion[4]
O/H (x 10^4)	5.5±1.5	4.8±2.0	4.4±.19	7.41	5.25
S/H (x 10^5)	0.69±.41	0.83±.82	1.1±.085	2.14	1.48
S/O (x 10^1)	0.13±.073	0.17±.14	0.25±.022	0.29	0.28
Cl/H (x 10^7)	1.9±1.1	$\cdots$	2.1±.18	3.16	2.14
Cl/O (x 10^3)	0.33±.15	$\cdots$	0.47±.04	0.43	0.41
Ar/H (x 10^6)	2.8±1.2	2.5±2.5	2.9±.19	3.31	3.09
Ar/O (x 10^2)	0.51±.18	0.48±.48	0.69±.05	0.45	0.59

[1]Average abundance ratios for a sample of planetary nebulae from Kingsburgh & Barlow (1994)

[2]Average abundance ratios for a sample of planetary nebulae from Aller & Keyes (1987)

[3]Grevesse et al. (1996)

[4]Esteban et al. (1998), Table 19, gas + dust

REFERENCES

Acker, A., Ochsenbein, F., Stenholm, B., Tylenda, R., Marcout, J., & Schohn, C. 1992, The Strasbourg-ESO Catalogue of Galactic Planetary Nebulae (Garching: ESO)

Aldrovandi, S.M.V., & Péquignot, D. 1973, A&A, 25, 137

Ali, B., Blum, R.D., Bumgardner, T.E., Cranmer, S.R., Ferland, G.J., Haefner, R.I., & Tiede, G.P. 1991, PASP, 103, 1182

Aller, L.H., & Czyzak, S. 1983, ApJS, 51, 211

Aller, L.H., & Keyes, C.D. 1987, ApJS, 65, 405

Baluja, K.L., & Zeippen, C.J. 1988, J. Phys. B, 21, 1455

Barker, T., 1978a, ApJ, 220, 193

——. 1978b, ApJ, 221, 145

——. 1980a, ApJ, 237, 482

——. 1980b, ApJ, 240, 99

——. 1983, ApJ, 270, 641

Bhatia, A. K., & Kastner, S. O. 1995, MNRAS, 272, 311

Burke, V.M., Lennon, D.J., & Seaton, M.J. 1989, MNRAS, 236, 353

Butler, S.E., & Dalgarno, A. 1980, ApJ, 241, 838

Butler, K., & Zieppen, C.J. 1989, A&A, 208, 337

——. 1994, A&AS, 107, 1

Cappellaro, E. Evans, R., & Turatto, M. 1999, A&A, 351, 459

Chapman, R.D., & Henry, R.J.W. 1971, ApJ, 168, 169

Clegg, R. 1987, MNRAS, 229, 31p

Dennefeld, M., & Stasińska, G. 1983, A&A, 118, 234

Dinerstein, H., 1980, ApJ, 237, 486

Esteban, C., Peimbert, M., Torres-Peimbert, S., & Escalante, V. 1998, MNRAS, 295, 401

Ferland, G.J. 1996, *Hazy, A Brief Introduction to Cloudy*, University of Kentucky Department of Physics & Astronomy Internal Report

Freitas-Pacheco, J.A 1993, ApJ, 403, 673

Freitas-Pacheco, J.A., Maciel, W.J., & Costa, R.D.D. 1992, A&A, 261, 579

French, H.B. 1981, ApJ, 246, 434

Galavís, M.E., Mendoza, C., & Zeippen, C.J. 1995, A&AS, 111, 347

Garnett, D.R. 1989, ApJ, 345, 282

Garnett, D.R., & Dinerstein, H. 2001, ApJ, in press (astro-ph/0105206)

Grevesse, N., Noels, A., & Sauval, A.J. 1996, in ASP Conf. Ser. 99 , Cosmic Abundances, ed. S.S. Holt & G. Sonneborn (San Francisco: ASP), 117

Henry, R.B.C., Kwitter, K.B., & Bates, J.A. 2000, ApJ, 531, 928

Henry, R.B.C., Kwitter, K.B., & Howard, J.W. 1996, ApJ, 458, 215

Henry, R.B.C., & Worthey, G. 1999, PASP, 111, 919

van den Hoek, L.B., & Groenewegen, M.A.T. 1997, A&AS, 123, 305

Hyung, S., Aller, L.H., Feibelman, W.A., & Lee, W.-B. 2001, ApJ, in press

Kingsburgh, R.L., & Barlow, M.J. 1994, MNRAS, 271, 257

Köppen, J.A., Acker, A., & Stenholm, B. 1991, A&A, 248, 197

Kwitter, K.B., & Henry, R.B.C. 1996, ApJ, 473, 304

——. 1998, ApJ, 493, 247

Lennon, D.J., & Burke, V.M. 1994, A&AS, 103, 273

Maciel, W.J., & Chiappini, C. 1994, Ap&SS, 219, 231

Maciel, W.J., & Köppen, J. 1994, A&A, 282, 436

Maciel, W.J., & Quireza, C. 1999, A&A, 345, 629

Maeder, A. 1992, A&A, 264, 105

Marigo, P., Bressan, A., & Chiosi, C. 1998, A&A, 331, 564

Mathis, J.S., Torres-Peimbert, S., & Peimbert, M. 1998, ApJ, 495, 328

McLaughlin, B.M., & Bell, K. L. 1993, ApJ, 408, 753

Mendoza, C. 1983, in IAU Symp. 103, *Planetary Nebulae*, ed. D.R. Flower, Dordrecht: Reidel, 143.

Mendoza, C., & Zeippen, C.J. 1983, MNRAS, 202, 981

——. 1982, MNRAS, 198, 127

Natta, A., Panagia, N., & Preite-Martinez, A. 1980, ApJ, 242, 596

Nomoto, K., Hashimoto, M., Tsujimoto, T., Thielemann, F.-K., Kishimoto, N., Kubo, Y., & Nakasato, N. 1997a, Nuc. Phys. A, 616, 79c

Nomoto, K., Iwamoto, K., Nakasato, N., Thielemann, F.-K., Brachwitz, F., Tsujimoto, T., Kubo, Y., & Kishimoto, N. 1997b, Nuc. Phys. A, 621, 467c

Osterbrock, D.E. 1989, *Astrophysics of Gaseous Nebulae and Active Galactic Nuclei*, (Mill Valley, CA: University Science Books)

Pagel, B.E.J. 1978, MNRAS, 183, 1p

Peimbert, M. 1990, Rep. Prog. Phys., 53, 1559

Peimbert, M., & Costero, R. 1969, Bol. Obs. Tonantzintla y Tacubaya, 5, 3

Peimbert, M., Luridiana, V., & Torres-Peimbert, S. 1995, Rev. Mex. Astron. y Astrof. Ser. Conf., Vol. 3, The Fifth Mexico-Texas Conference on Astrophysics: Gaseous Nebulae and Star Formation, p. 295

Peimbert, M., & Torres-Peimbert, S. 1987, Rev. Mex. Astron. Astrofis., 14, 540

Péquignot, D., Petitjean, P., & Boisson, C. 1991, A&A, 251, 680

Ramsbottom, C.A., Bell, K.L., & Stafford, R.P. 1996, Atom. Dat. Nuc. Dat. Tab. 63, 57

Savage, B.D., & Mathis, J.S. 1979, ARA&A, 17.73

Seaton, M. J., Zeippen, C. J., Tully, J. A., Pradhan, A. K., Mendoza, C., Hibbert, A. 1992, Rev. Mex. Astr. Astrofis., 23, 19 Berrington, K. A.

Stasińska, G. 1978, A&A, 66, 257

——. 1982, A&AS, 48, 299

——. 1998, in ASP Conf. Ser. 147, Abundance Profiles: Diagnostic Tools for Galaxy History, ed. D. Friedli, M. Edmunds, C. Robert, & L. Drissen (San Francisco: ASP), 142

Stevenson, C.C. 1994, MNRAS, 267, 904

Storey, P. J., & Hummer, D. G. 1995, MNRAS, 272, 41

Verner, D.A., Ferland, G.J., Korista, K.T., & Yakovlev, D.G. 1996, ApJ, 465, 487

Wiese, W.L., Fuhr, J.R., & Deters, T.M. 1996, in Atomic Transition Probabilities of Carbon, Nitrogen, and Oxygen : A Critical Data Compilation, Amer. Chem. Soc., Washington, D.C.

Woosley, S.E., & Weaver, T.A. 1995, ApJS, 101, 181

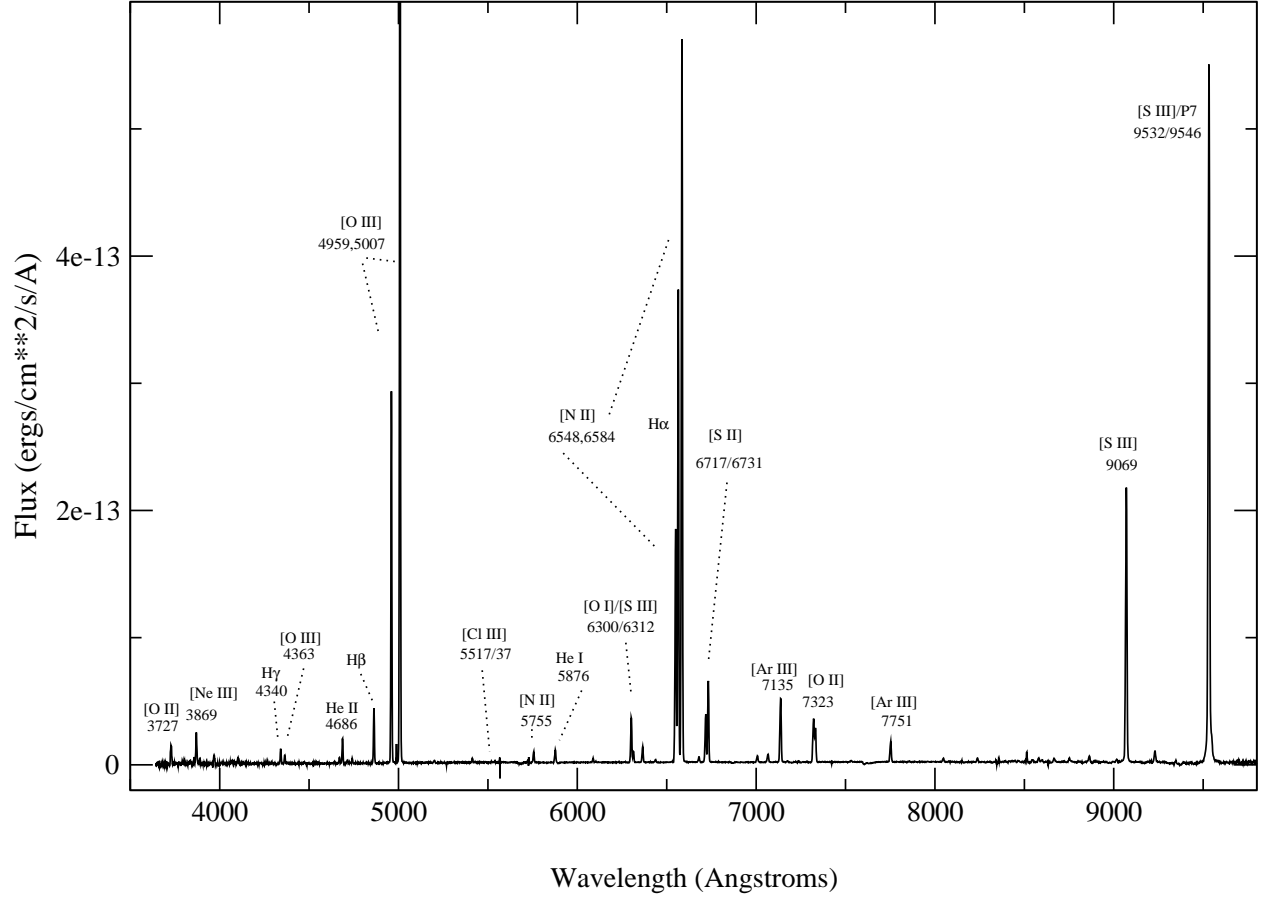Zeippen, C.J., Le Bourlot, J., & Butler, K. 1987, A&AS, 188, 251

Fig. 1.— Spectrum of M1-57, produced by merging blue and red spectra observed for the object. Important emission lines used to determine diagnostics and abundances are indicated.
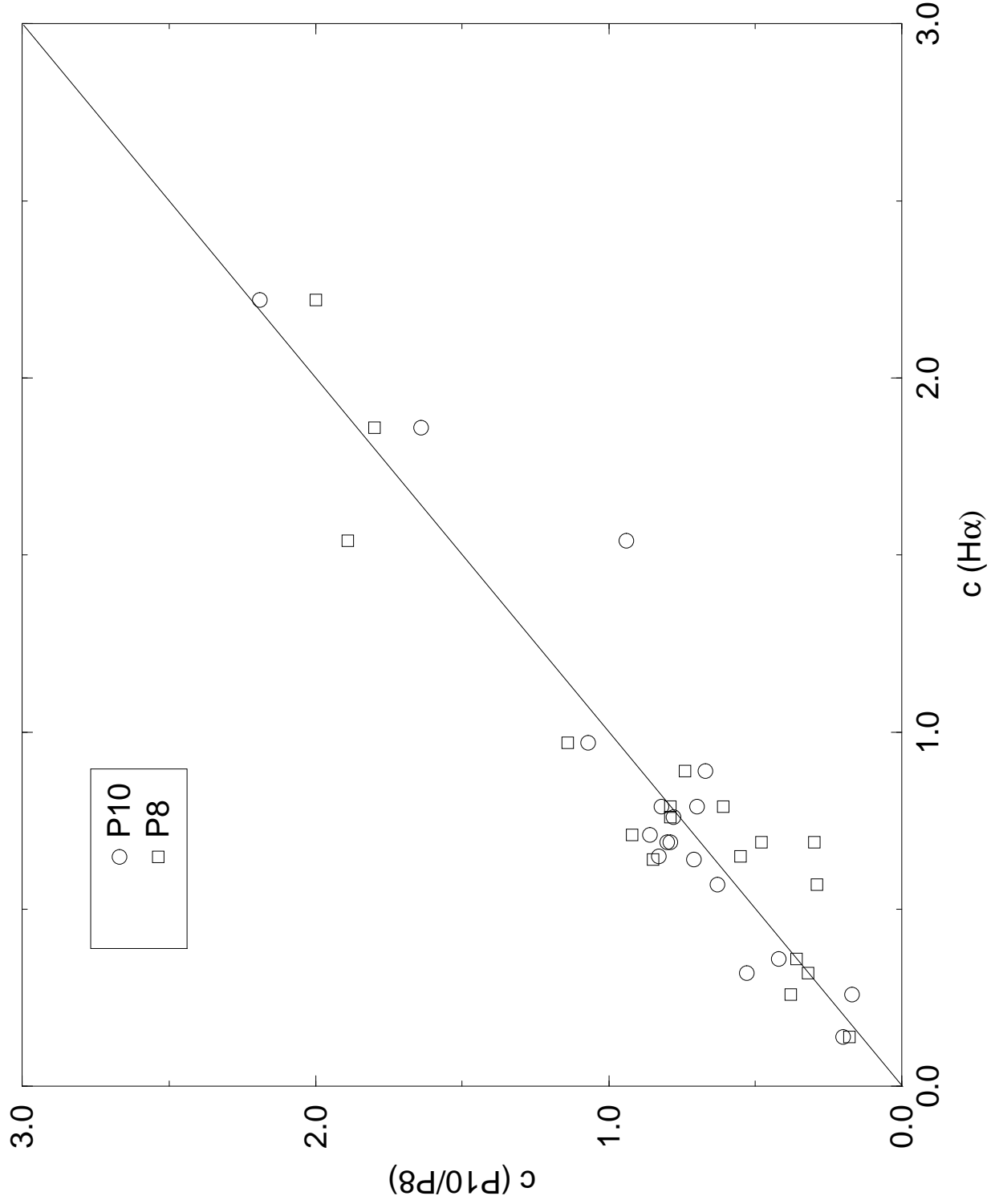
Fig. 2.— A comparison of logarithmic extinction c as determined using the Paschen 8 and 10 lines versus the value inferred from using Hα. The solid line shows the track for a one-to-one correspondence.
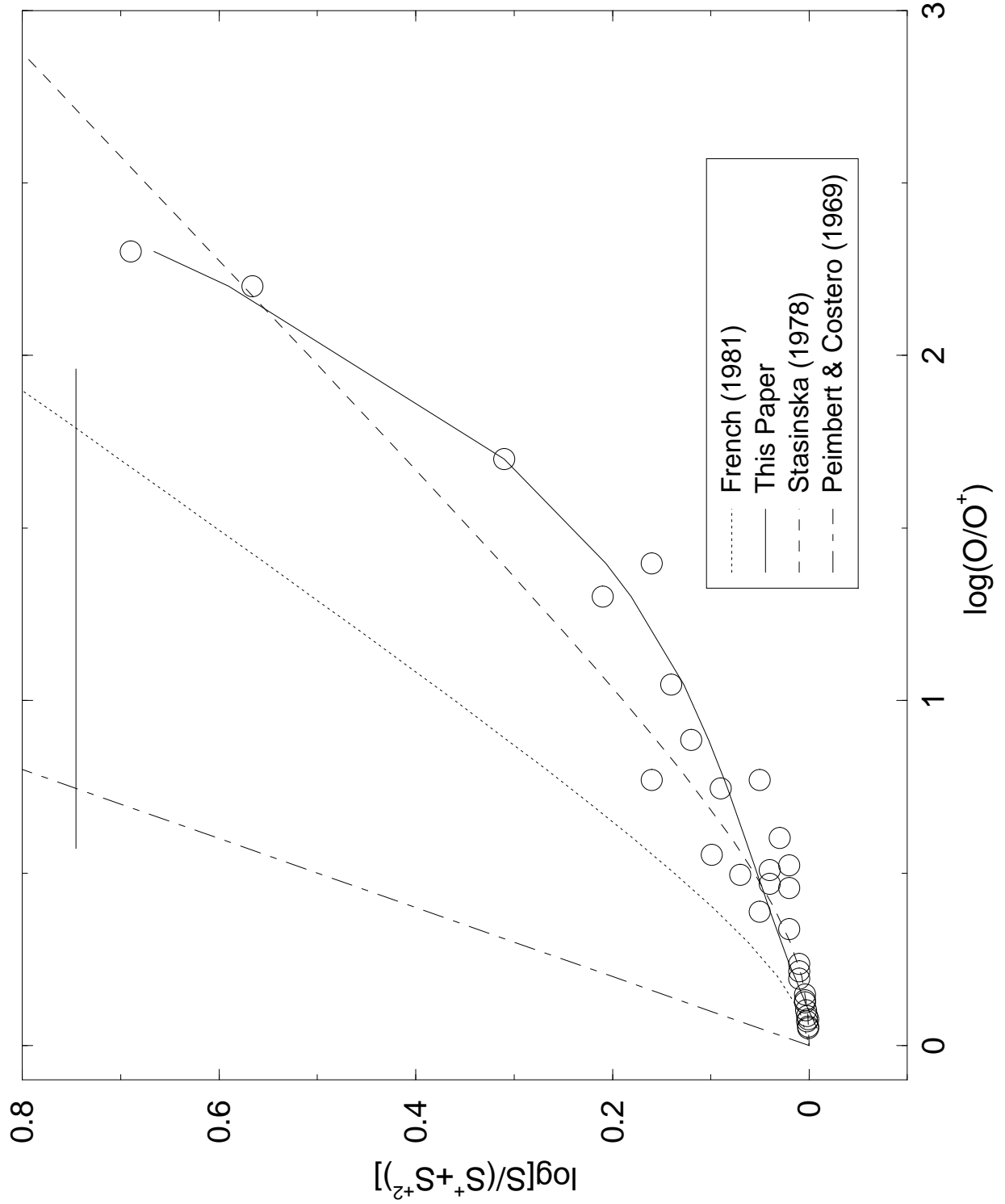
Fig. 3.— Logarithmic ratios of the elemental S abundance relative to the sum of S^+ and S^{+2} ionic abundances vs. elemental O to the O^+ ionic abundance from predictions of photoionization models spanning a range in stellar effective temperature, nebular density, and matter-boundedness, as discussed in the text. Each circle represents one model. The solid horizontal line at the top of the graph shows the range of our observed values of O/O^+. The solid curve is our third order fit whose coefficients are given in the text, while the dot-dashed, dotted and dashed lines correspond to relations developed by Peimbert & Costero (1969), French (1981) and Stasińska (1978), respectively.
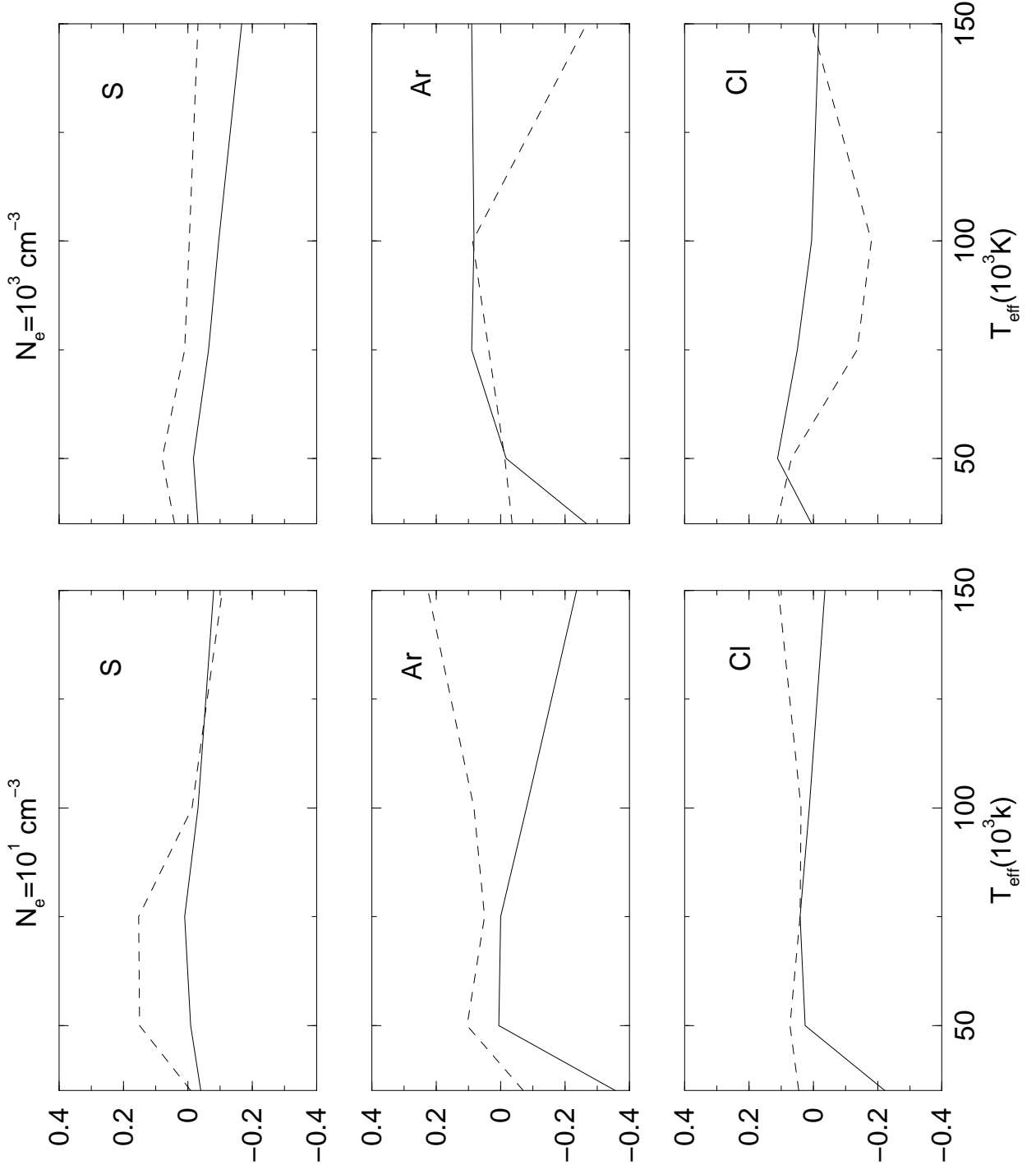
Fig. 4.— Logarithmic ratio of model elemental abundance inferred by ABUN relative to the actual model input abundance for S, Ar, and Cl, vs. model stellar effective temperature. Plots on the left and right are for nebular densities of 10 and 1000 cm^{-3}, respectively. Solid curves show track of models which extend out to 1 Strömgren radius, while the dashed lines show the same for models which are stopped at 0.5 Strömgren radius.
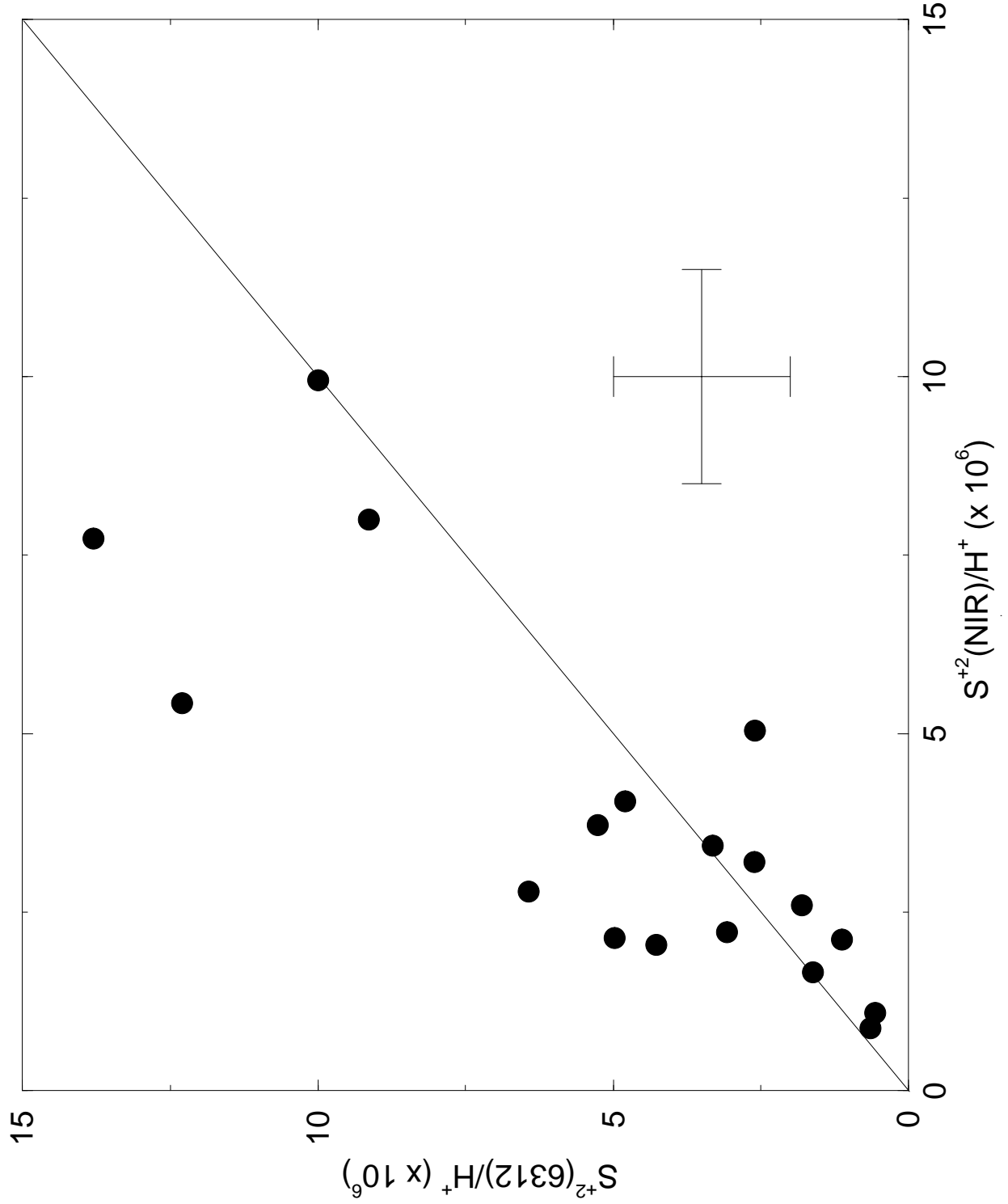
Fig. 5.— Comparison of S^{+2}/H^+ for S abundances computed using the 6312Å emission line along with the [N II] temperature (ordinate) and the NIR emission lines along with the [S III] temperature (absissa). The solid line shows the track of a one-to-one correspondence.
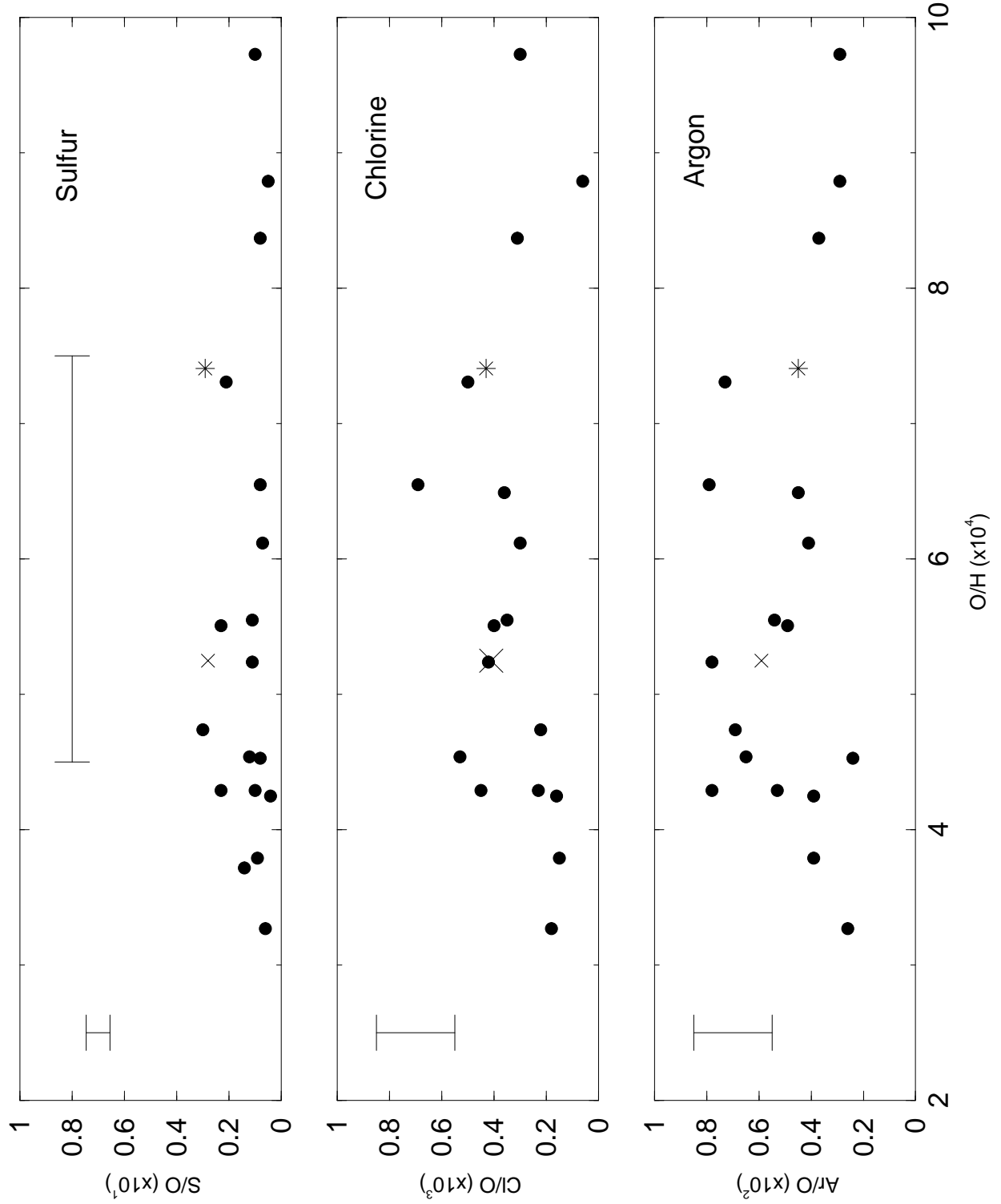
Fig. 6.— Top: S/O (x 10^1) versus O/H (x 10^4), where filled circles are ratios determined in this paper. The position of the sun (Grevesse et al. 1996) and the Orion nebula (Esteban et al. 1998) are indicated with a star and an X, respectively. Middle: Same as top but for Cl/O (x 10^3). Bottom: Same as top but for Ar/O (x 10^2). Ordinate uncertainties are shown with error bars in each panel, while the horizontal error bar in the top panel shows the O/H uncertainty for all three panels.